JVI Journals.ASM.org

Genome-Wide DNA Methylation as an Epigenetic Consequence of Epstein-Barr Virus Infection of Immortalized Keratinocytes

Christine E. Birdwell,[b,c] Krista J. Queen,[b,c]* Phillip C. S. R. Kilgore,[a] Phoebe Rollyson,[d] Marjan Trutschl,[a] Urska Cvek,[a] Rona S. Scott[b,c,e]

Department of Computer Science, Louisiana State University—Shreveport, Shreveport, Louisiana, USA[a]; Department of Microbiology and Immunology,[b] Center for Molecular and Tumor Virology,[c] Department of Biochemistry,[d] and Feist-Weiller Cancer Center,[e] Louisiana State University Health Sciences Center—Shreveport, Louisiana, USA

ABSTRACT

The oral cavity is a persistent reservoir for Epstein-Barr virus (EBV) with lifelong infection of resident epithelial and B cells. Infection of these cell types results in distinct EBV gene expression patterns regulated by epigenetic modifications involving DNA methylation and chromatin structure. Regulation of EBV gene expression relies on viral manipulation of the host epigenetic machinery that may result in long-lasting host epigenetic reprogramming. To identify epigenetic events following EBV infection, a transient infection model was established to map epigenetic changes in telomerase-immortalized oral keratinocytes. EBV-infected oral keratinocytes exhibited a predominantly latent viral gene expression program with some lytic or abortive replication. Calcium and methylcellulose-induced differentiation was delayed in EBV-positive clones and in clones that lost EBV compared to uninfected controls, indicating a functional consequence of EBV epigenetic modifications. Analysis of global cellular DNA methylation identified over 13,000 differentially methylated CpG residues in cells exposed to EBV compared to uninfected controls, with CpG island hypermethylation observed at several cellular genes. Although the vast majority of the DNA methylation changes were silent, 65 cellular genes that acquired CpG methylation showed altered transcript levels. Genes with increased transcript levels frequently acquired DNA methylation within the gene body while those with decreased transcript levels acquired DNA methylation near the transcription start site. Treatment with the DNA methyltransferase inhibitor, decitabine, restored expression of some hypermethylated genes in EBV-infected and EBV-negative transiently infected clones. Overall, these observations suggested that EBV infection of keratinocytes leaves a lasting epigenetic imprint that can enhance the tumorigenic phenotype of infected cells.

IMPORTANCE

Here, we show that EBV infection of oral keratinocytes led to CpG island hypermethylation as an epigenetic scar of prior EBV infection that was retained after loss of the virus. Such EBV-induced epigenetic modification recapitulated the hypermethylated CpG island methylator phenotype (CIMP) observed in EBV-associated carcinomas. These epigenetic alterations not only impacted gene expression but also resulted in delayed calcium and methylcellulose-induced keratinocyte differentiation. Importantly, these epigenetic changes occurred in cells that were not as genetically unstable as carcinoma cells, indicating that EBV infection induced an epigenetic mutator phenotype. The impact of this work is that we have provided a mechanistic framework for how a tumor virus using the epigenetic machinery can act in a "hit-and-run" fashion, with retention of epigenetic alterations after loss of the virus. Unlike genetic alterations, these virally induced epigenetic changes can be reversed pharmacologically, providing therapeutic interventions to EBV-associated malignancies.

Epstein-Barr virus (EBV) is a prevalent gammaherpesvirus infecting greater than 90% of adults worldwide. EBV has tropism for both epithelial cells, where the virus is thought to undergo lytic replication, and B cells, where the virus can establish a lifelong latent infection. Initial infection is usually asymptomatic, although infection later in life is associated with an increased risk for the development of infectious mononucleosis. EBV is also associated with a number of B cell and epithelial cell malignancies characterized by having a latent viral infection.

In order to establish latency and the lifelong carrier state, EBV utilizes a series of increasingly strict latency gene expression programs in order to drive B cells into long-lived memory cells and evade the immune system (1). Reactivation of the virus occurs upon terminal B cell differentiation, with the epithelium supporting additional viral replication to propagate the cycle of persistence. The various EBV gene expression states have been shown to involve changes in viral gene expression and promoter usage that are regulated by epigenetic modifications to the viral genome that result from viral manipulation of the host epigenetic machinery (2–4).

Epigenetic modifications are defined as heritable gene expression states that occur without altering the DNA sequence. Epigenetic mechanisms include DNA methylation and histone modifi-

Received 6 April 2014 Accepted 15 July 2014
Published ahead of print 23 July 2014
Editor: R. M. Longnecker
Address correspondence to Rona S. Scott, rscott1@lsuhsc.edu.
* Present address: Krista J. Queen, Gastroenteritis and Respiratory Viruses Laboratory Branch, Centers for Disease Control and Prevention, Atlanta, Georgia, USA.
Supplemental material for this article may be found at http://dx.doi.org/10.1128/JVI.00972-14.

doi:10.1128/JVI.00972-14

cations, both of which regulate EBV's life cycle. Inside the virion, the linear EBV genome is essentially devoid of epigenetic modifications (5, 6), but upon entering the host cell, the viral DNA genome circularizes and quickly becomes methylated and histone associated (reviewed in reference 4). DNA methylation of both the viral genome and the host genome is carried out by the cellular DNA methyltransferases (DMNTs) 1, 3A, or 3B. DNMT1 is associated with maintenance methylation of the host genome during replication while DNMT3A and -B are associated with *de novo* methylation. In type I latently infected B cells, exhibiting the most restricted viral gene expression program, treatment with the DNMT inhibitor 5-azacytidine can reverse the methylation of Wp, Cp, and latent membrane protein (LMP) promoters and restore EBV nuclear antigen (EBNA) and LMP expression (7, 8). Although the regulatory mechanisms that guide viral DNA methylation have not been fully delineated, EBV-encoded LMPs have been reported to increase the expression levels or activity of all three cellular DNMTs (3, 9, 10). DNA methylation is also involved in regulation of lytic gene expression as the viral lytic switch transcription factor BZLF1 binds preferentially to methylated DNA (11, 12). Chromatin structure and modifications also participate in the regulation of EBV gene expression. The chromatin insulator CCCTC-binding factor has several binding sites on the EBV genome, and mutation of these sites results in aberrant EBV gene expression (2, 13). Additionally, EBNA2 interacts with histone acetyltransferases to activate viral promoters, whereas EBNA3 can inhibit EBNA2 promoter transactivation by recruiting repressive chromatin complexes (reviewed in reference 4).

EBV manipulation of the host epigenetic machinery has effects on the host epigenome as well, which is apparent in EBV-associated malignancies and provides a framework for viral "hit-and-run" oncogenesis (14). EBV-positive nasopharyngeal and gastric carcinomas exhibit a high frequency of CpG island (CGI) hypermethylation (CpG island methylator phenotype [CIMP]) at various tumor suppressor genes (9, 15–21). Furthermore, expression of LMP1 and LMP2A viral oncoproteins has been shown through induction of the host DNMTs to result in hypermethylation and silencing of E-cadherin and PTEN tumor suppressor promoter regions, respectively (9, 10, 22). EBV-associated epigenetic alterations to the host genome are not limited to DNA methylation. The EBNA3 proteins recruit polycomb group complexes to the Bim and p16 cellular promoters, reducing gene expression through repressive histone modifications (23–25). In contrast, B cell immortalization by EBV resulted in large-scale hypomethylation that affected two-thirds of the B cell genome. Promoter hypomethylation of a number of proliferative genes was consistent with the conversion of resting B cells to proliferating blasts (26, 27). EBV infection of germinal center B cells not only was shown to alter DNMT expression, resulting in changed DNA methylation patterns at particular regions, but also induced the histone 3 lysine 27 demethylase, KDM6B, potentially regulating genes differentially expressed in Hodgkin's lymphoma (28, 29). However, in carcinoma cells, we previously demonstrated that EBV infection led to epigenetic silencing at the PYCARD and E-cadherin gene loci involving DNA methylation and repressive chromatin modifications, respectively (30). Importantly, these epigenetic changes were maintained following loss of the virus and indicated that their heritable nature was not dependent on continued viral gene expression (30). A limitation of studies using cancer cells is the propensity for genomic instability that results in complex genetic and epigenetic changes that may confound epigenetic events induced by EBV infection. Cancer cells, including the carcinoma cells used in our previous study, may also acquire or tolerate virally induced epigenetic changes that might not occur in normal cells. Thus, we examined the epigenetic consequences following EBV infection of immortalized normal oral keratinocytes (NOK) using our model of transient EBV infection. We found that NOK, like the carcinomas cells, showed evidence of EBV-induced epigenetic changes, as evidenced by phenotypic and transcriptional changes in infected cells that were retained after loss of the virus. DNA methylation analysis demonstrated increased CpG island hypermethylation in EBV-infected cells, an event documented to occur in EBV-associated carcinomas. These methylation events correlated with gene expression changes, some of which could be partially restored by treatment with the DMNT inhibitor, decitabine (DAC). Overall, these observations suggest that EBV uses epigenetic modifications to control aspects of its viral life cycle with effects to the host genome either directly to benefit the virus or indirectly as a result of manipulation of the host epigenetic machinery. Regardless, the effects of these changes would have long-term consequences and be maintained with minimal or no viral gene expression.

MATERIALS AND METHODS

Cell culture. Human telomerase (hTERT)-immortalized normal oral keratinocytes (NOK; kindly gifted by Karl Munger) were cultured in keratinocyte serum-free medium (KSFM) supplemented with human epidermal growth factor and bovine pituitary extract (Life Technologies). A clonal population derived from the NOK cell line was infected by coculture for 24 h with anti-IgG-induced Akata BL cells carrying a recombinant EBV containing neomycin resistance and green fluorescent protein (GFP) expression cassettes in place of the BXLF1 gene. After removal of the B cells, infected cells were selected with 350 μg per milliliter of G418 (Corning Cellgro). Clonal outgrowths appeared after 3 weeks and were on selection for 10 passages. To generate transiently infected clones, selection pressure was removed for an additional 10 passages, followed by flow-cytometric single-cell cloning. EBV positivity of infected and transiently infected cells was confirmed by EBV encoded RNA (EBER) *in situ* hybridization (ISH). As controls, uninfected parental cells were transfected with PTRUF5 plasmid (kind gift from Lindsey Hutt-Fletcher), which contains the GFP and neomycin resistance cassettes used to generate the recombinant virus (31). NOK were transfected using a Nucleofector I system (Amaxa) using primary mammalian epithelial cell solution (VPI-1005; Lonza) and program S05. Both uninfected parental cells and plasmid-transfected controls were cultured using a method similar to that of the infected cells and were single-cell sorted. DNA fingerprinting analysis was used to authenticate the identity of cell clones with respect to the uninfected parental controls (32).

Genomic PCR and Southern blotting. To validate EBV loss and exclude the possibility of viral integration, DNA PCR or Southern blotting was used. For genomic PCR, 100 nanograms of DNA from uninfected, vector, EBV-positive, and three EBV-negative transiently infected clones was amplified by a series of primers spanning the entire EBV genome (see Table S1 in the supplemental material). Amplicons were electrophoresed on 1× TAE (Tris-acetate EDTA)-agarose gels and visualized by ethidium bromide staining. To determine the limits of detection, serial 10-fold dilutions of Namalwa DNA, a B cell line with two integrated copies of EBV, were used. Southern blotting was performed as previously described (33). Briefly, 30 μg of total cellular DNA was digested overnight with the restriction enzyme BamHI, loaded onto a 1× TBE (Tris-borate-EDTA)-agarose gel, and electrophoresed overnight. Fragments larger than 1.6 kb were treated with 0.2% HCl for 15 min and were washed in denaturing buffer for 20 min, followed by a 20-min wash in neutralizing buffer. The

gel was transferred to a nylon membrane overnight by capillary action. Transferred DNA was UV cross-linked (Bio-Rad GS Gene Linker UV chamber; 150 mJ) to the membrane and hybridized overnight in buffer containing 6× SSC (1× SSC is 0.15 M NaCl plus 0.015 M sodium citrate), 10× Denhardt's, 50% formamide, 1% SDS, and 0.1 mg/ml sheared calf thymus DNA (Trevigen) with 1×10^6 cpm/ml of a radiolabeled probe corresponding to the EcoRI A or the BamHI NJhet fragment of the EBV genome. Hybridized membranes were visualized by autoradiography.

Immunofluorescence. Approximately 20,000 cells were seeded into each well of an eight-well glass chamber slide (Lab-Tec) in 0.2 ml of KSFM. After 48 h, cells were fixed in cold 4% paraformaldehyde for 15 min at room temperature, washed with Dulbecco's phosphate-buffered saline (PBS), and permeabilized for 10 min with 0.2% Triton X-100 in PBS. Slides were washed three times with PBS and incubated in 5% goat serum to block nonspecific binding for 30 min at room temperature. A 1:50 dilution of anti-EBNA1 antibody (OT-1x; kind gift of Martin Sapp) was added, and slides were incubated overnight at 4°C in a humidified chamber. Following three PBS washes, slides were incubated with a 1:1,000 dilution of Alexa 546 anti-mouse (Invitrogen) for 1 h at 37°C in a humid chamber protected from light. After a final three washes in PBS, slides were allowed to air dry protected from light. Mounting medium containing 4′,6′-diamidino-2-phenylindole (DAPI; Vector) was added, and pictures were acquired at ×20 magnification on an Olympus Bx50 fluorescence microscope equipped with a SenSys camera and Metaview software. Final images were further analyzed with ImageJ (National Institutes of Health) software.

RT-PCR. For EBV gene expression profiling of infected NOK, reverse transcription-PCR (RT-PCR) was used. Total cellular RNA was harvested in RNA STAT60 (Tel-Test, Friendswood, TX) and purified per the manufacturer's instructions. Ten micrograms of total RNA was used to make cDNA as previously described (30). One hundred nanograms of cDNA was amplified using Go *Taq* DNA Polymerase (1 unit/reaction; Promega), 5× Go *Taq* buffer (Promega), 500 nM specific primer (see Table S1 in the supplemental material), and 200 nM each deoxynucleoside triphosphate (dNTP) (Illustra dNTP Polymerization Mix; GE Healthcare). PCR was run for 5 min at 94°C, followed by 35 to 40 cycles of 94°C, 60°C, and 72°C for 30 s each before a 7-min final extension period at 72°C. Primers and melting temperature (T_m) conditions are described in Table S1. PCR products were electrophoresed on 2% agarose gels and visualized by ethidium bromide staining.

Cell proliferation assay. A total of 1,000 cells per well were seeded in 96-well plates (BD Falcon) in triplicate. At 24, 48, 72, and 96 h postseeding, 20 μl of Promega CellTiter 96 AQueous One Solution was added and incubated at 37°C for 2 h before being read on a FLUstar Omega (BMG Labtech) plate reader at 490 nm.

Transepithelial electrical resistance. Corning 0.33-cm^2 Transwell inserts were seeded with 3.3×10^4 cells per insert in duplicate and allowed to form monolayers over a week. Once monolayers had formed, cells were cultured in KSFM containing 1 to 1.5 millimolar calcium chloride to induce differentiation and the formation of polarized layers. Transepithelial electrical resistance (TEER) was measured with a Millipore Millicell-ERS (electrical resistance system) with the 2,000-Ω-range setting three times per insert. Measurements were taken daily prior to changing the medium. Background was accounted for by measuring the resistance of empty inserts in medium, also in duplicate, and subtracting that average value from the average value of the resistance measurements for the inserts containing the cell lines. Resistance values corrected for background were then multiplied by the area of the insert ($\Omega \times cm^2$).

Methylcellulose-induced differentiation. Methylcellulose (Sigma) was prepared in KSFM plus supplements (5 ng/ml epidermal growth factor [EGF] and 50 μg/ml bovine pituitary extract) as previously described (34). A total of 2×10^6 cells were suspended in 10 ml of the 1.5% methylcellulose solution and incubated for 24 h at 37°C. Methylcellulose was removed by PBS washes, and the cell pellet was lysed with RNA STAT60. As an undifferentiated control, 10^6 cells were seeded in a 60-mm-diameter tissue culture dish, and RNA was harvested after 24 h. Ten micrograms of RNA was used to make cDNA as previously described. Twenty nanograms of cDNA was used in quantitative real-time PCR as described below relative to the cellular housekeeping gene cyclophilin A as a normalization control. Primers used are listed in Table S1 in the supplemental material.

RRBS. Reduced representation bisulfite sequencing (RRBS) and bioinformatic analysis were carried out by Zymo Research Corporation (Epiquest Service) on an uninfected clone, a vector control, an EBV-positive clone, and three EBV-negative transiently infected clones. Briefly, RRBS libraries were prepared from 200 to 500 nanograms of genomic DNA digested with TaqI and MspI sequentially and then size selected (40 to 350 bp) and 3′-terminal A extended. Ligation to preannealed adaptors containing 5′-methyl-cytosine instead of cytosine (Illumina) was performed using an Illumina DNA preparation kit and protocol. Purified, adaptor-ligated fragments were bisulfite treated using an EZ DNA Methylation-Direct kit (Zymo Research). Preparative-scale PCR was performed, and DNA Clean and Concentrator-purified PCR products were subjected to a final size selection on a 4% NuSieve 3:1 agarose gel. SYBR green-stained gel slices containing adaptor-ligated fragments ranging from 130 to 460 bp in size were excised. Library material was recovered from the gel (Zymoclean Gel DNA Recovery kit) and sequenced on an Illumina HiSeq platform.

Sequence alignments and data analysis. Sequence reads from bisulfite-treated EpiQuest libraries were identified using standard Illumina base-calling software and then analyzed using a Zymo Research proprietary analysis pipeline. Residual cytosines (Cs) in each read were first converted to thymines (Ts), with each such conversion noted for subsequent analysis. A reference sequence database was constructed from the 50-bp ends of each computationally predicted MspI-TaqI fragment in the 40- to 350-bp size range. All Cs in each fragment end were then converted to Ts (only the C-poor strands are sequenced in the RRBS process); Bowtie was used to align the converted reads to the converted reference. The number of mismatches in the induced alignment was then counted between the unconverted read and reference, ignoring cases in which a T in the unconverted read was matched to a C in the unconverted reference. For a given read, the best alignment was kept if the second-best alignment had two or more mismatches; otherwise, the read was discarded as nonunique. The methylation level of each sampled cytosine was estimated as the number of reads reporting a C, divided by the total number of reads reporting a C or T. Fisher's exact test or a *t* test was performed for each CpG site which had at least five reads covered. Also, promoter, gene body, and CpG island annotations were added to each CpG. The software pipeline is implemented in Python. A similar approach was used to align reads to the Akata EBV genome (KC207813) (35). For methylation level analysis, CpG residues covered by five or more reads were used. Unmethylated CpGs were considered in reads having 0 to 20% methylation, while methylated CpGs were considered in reads with 50 to 100% methylation. The methylation status of the viral genome in the EBV-positive clone was visualized using Circos (36).

Microarray transcriptional profiling. Uninfected parental cells, a vector control, EBV-infected clones, and EBV-negative transiently infected clones were seeded at 1×10^6 cells in a T75 flask. RNA was harvested 3 days after seeding using STAT60 (Tel-Test) according to the recommended protocol. Transcriptional profiles from duplicate seedings of cells were determined as previously described (30). Fifteen micrograms of fragmented, biotin-labeled cRNA was hybridized to Affymetrix U133 Plus 2.0 GeneChips. Microarrays were scanned using a GeneChip Scanner 3000, and intensity values were determined and analyzed using Gene Chip Operating Software (GCOS), version 1.4 (Affymetrix). Gene expression calls and data were analyzed in GeneSifter. First, statistically significant gene expression values were identified between each sample, yielding approximately 5,500 genes that were used in principal component analysis (PCA). Second, pairwise comparisons between RNA samples from cells exposed to EBV (three EBV-negative transiently infected clones and an EBV-positive clone) and uninfected controls (uninfected parental and

vector transfected control cells) generated a filtered gene list based on a quality score of 0.5, statistical significance (analysis of variance [ANOVA], $P < 0.05$), and a fold change cutoff of 1.8.

DAC treatment and real-time reverse transcription-PCR. A total of 2×10^5 NOK (uninfected, vector, and EBV-positive [EBV$^+$] clones and three EBV-negative transiently infected clones) were seeded in T-25 flasks and treated with either 1 μM decitabine (DAC [5-aza-2′-deoxycytidine]) or an equal volume of dimethyl sulfoxide (DMSO) as a vehicle control for 96 h. The medium was changed, and fresh DAC or DMSO was added at 48 h. RNA was collected by STAT60 and purified according to the manufacturer's instructions. Ten micrograms of RNA was used to make cDNA by random priming and Moloney murine leukemia virus (MMLV) reverse transcription as previously described (33). Quantitative real-time reverse transcription-PCR (qRT-PCR) was performed on a 7500 FAST Applied Biosystems thermocycler using Power SYBR green (Life Technologies), 50 ng of cDNA, and 300 nM each primer in each reaction mixture. Primers are described in Table S1 in the supplemental material. Relative RNA levels were determined by using standard curve analysis based on serially diluted cDNA derived from uninfected NOK cells. The cellular housekeeping gene human hypoxanthine-guanine phosphoribosyltransferase (hHPRT) or cyclophilin A (peptidyl prolyl isomerase [PPIA]) was used as a normalization control. Negative controls included RT-negative and no-template water-only controls. RNA levels were reported relative to the level of the uninfected DMSO-treated NOK, which was arbitrarily set to 1.

Microarray data accession number. The genome methylation and microarray expression data have been deposited in Gene Expression Omnibus (GEO) under accession number GSE59843.

RESULTS

Generation of EBV-negative transiently infected clones. We have established a transient infection cell system to address the epigenetic consequences of EBV infection through loss of the viral episome in epithelial cells. As depicted in Fig. 1A, hTERT-immortalized NOK were infected via coculture with anti-IgG-induced Akata BL cells harboring a recombinant EBV strain where GFP and neomycin resistance cassettes replaced the EBV BXLF1 gene. Stably infected NOK cells were obtained by neomycin selection to force maintenance of the EBV episome. After 10 passages, selection pressure was removed to allow cells to naturally lose EBV episomes. EBV-negative transiently infected clones were identified by EBER ISH (Fig. 1B). To ensure complete loss of the viral episomes and the absence of viral integration, we profiled various regions of the EBV genome by PCR and Southern blotting (Fig. 1C to E). As shown in Fig. 1C, PCR amplification with primers that spanned the EBV genome in approximately 10-kb increments did not detect any EBV fragments in three EBV-negative transiently infected clones. However, robust amplification was observed in the EBV-positive clone and the Namalwa BL cell line possessing two integrated copies of EBV. As further evidence for the absence of any viral integration, we checked for remnants of the neomycin resistance cassette. The EBV-negative transiently infected clones became sensitive upon neomycin selection, similar to results with the uninfected controls (data not shown). Absence of the neomycin gene was confirmed by PCR in the three EBV-negative transiently infected clones, whereas stably transfected cells and EBV-positive cells as well as the vector control carrying the neomycin resistance cassette yielded the expected product (Fig. 1D). Moreover, Southern blotting examining the presence of the EBV internal W repeats (IRW) also failed to detect this repeated fragment in the three EBV-negative transiently infected clones with signal noted for the EBV-positive clone (Fig. 1E). Thus, these data indicate that we have successfully cured the infected NOK of EBV and generated a model system to examine true epigenetic consequences of EBV infection that do not rely on continued viral gene expression for their maintenance.

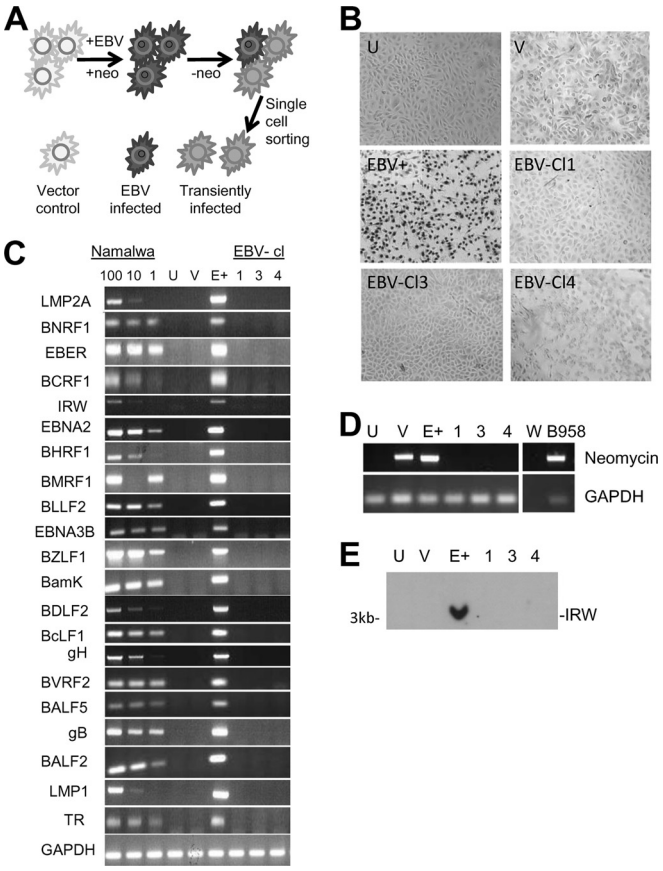

FIG 1 Transient infection of normal oral keratinocytes. (A) Schematic of transient infection of hTERT immortalized normal oral keratinocytes (NOK). A clonal NOK cell line was infected with a recombinant EBV (rEBV) carrying neomycin (neo) resistance and GFP cassettes in place of the BXLF1 gene. Neomycin selection pressure was applied to select and maintain EBV in the infected cell population. Removal of selection allowed loss of the viral episome (small black circles). Vector control indicates the clonal NOK cell line transfected with the PTRUF5 plasmid carrying the neomycin resistance and GFP cassettes. (B) *In situ* hybridization for EBV-encoded RNAs (EBERs) in uninfected, vector, EBV-positive and three EBV-negative transiently infected clones (EBV-cl1, EBV-cl3, and EBV-cl4). EBER positivity is indicated by dark nuclear staining in the EBV-positive cells. No EBER staining was detected in EBV-negative transiently infected clones. (C) DNA PCR spanning the viral genome in uninfected, vector, and EBV-positive (E+) clones and three EBV-negative transiently infected clones (EBV-cl 1, 3, and 4). The B cell line, Namalwa, with two integrated copies of EBV used as a limit of detection control at 100, 10, and 1 ng. (D) DNA PCR for the neomycin gene present in recombinant virus and vector plasmid. The EBV-positive cell line B958 was used as a positive control. Primers to glyceraldehyde-3-phosphate dehydrogenase (GAPDH) were used as a DNA loading control. (E) Southern blot for EBV genome using the EcoRI A fragment of the EBV genome as a probe in uninfected, vector, and EBV-positive clones and three transiently infected clones. U, uninfected; V, vector; E+, EBV-positive clone; 1, 3, and 4, transiently infected EBV-negative clones; W, water.

EBV infection epigenetically hindered keratinocyte differentiation. First, we characterized the viral gene expression program of the EBV-infected NOK cell line (Fig. 2A). Two independent EBV-infected cell lines (I1 and I2) and an EBV-positive clone derived from infection 1 were analyzed. RT-PCR analysis of latent

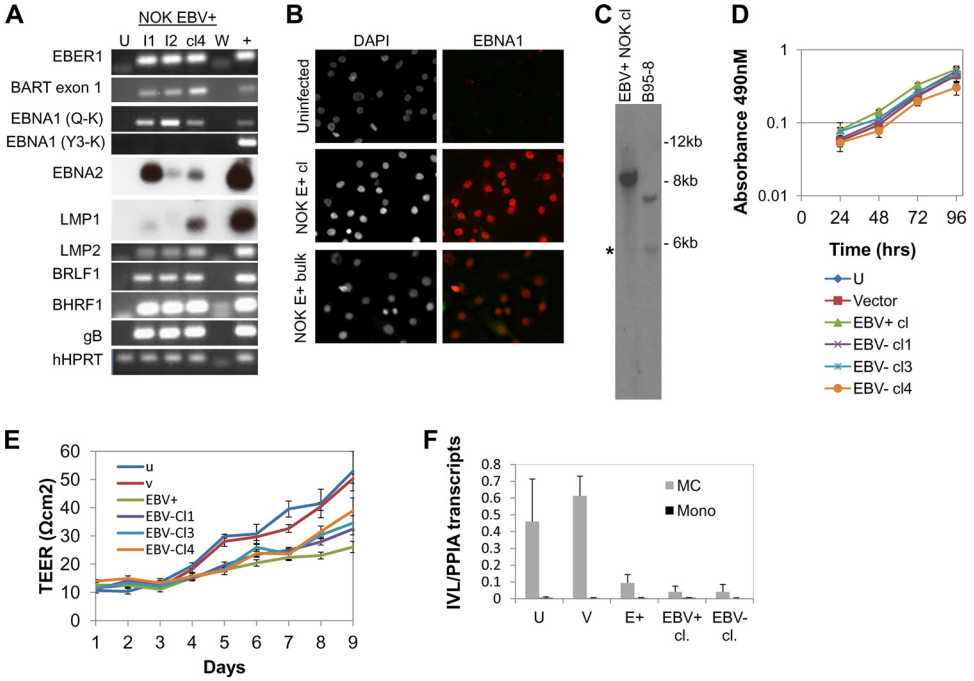

FIG 2 Characterization of EBV-infected and transiently infected EBV-negative NOK. (A) Reverse transcriptase PCR for detection of latent and lytic viral transcripts in an uninfected clone (U), EBV-infected cell lines 1 and 2 (I1 and I2, respectively), and an EBV-positive clone from I1 (clone 4, cl4). B958 (+) was used as a positive control. W indicates water as the template control. (B) EBNA1 immunofluorescence analysis. Cells shown in the left panels were stained with the nuclear stain DAPI; EBNA1-positive cells are shown in red in the right panels. NOK E+ bulk, EBV-positive NOK cell line. (C) Southern blotting for detection of fused and linear EBV terminal repeats probed with the BamHI NJhet fragment. The asterisk denotes end fragments from linear EBV DNA. (D) Cell proliferation using an MTS [3,4-(5-dimethylthiazol-2-yl)-5-(3-carboxymethoxy phenyl)-2-(4-sulfophenyl)-2H-tetrazolium salt] assay was measured at 24-h intervals for 96 h. Shown are the average absorbance values and standard errors of the means from three independent biological experiments. (E) Transepithelial electrical resistance following calcium-induced differentiation. Data are the averages and standard errors of the means from three independent biological experiments. Lower TEER measurements for EBV-positive and EBV-negative transiently infected clones were statistically significant relative to uninfected and vector controls starting at days 4 to 9. (F) Involucrin (IVL) expression following methylcellulose treatment. Cells were either seeded as a monolayer (mono) or suspended in methylcellulose for 24 h (MC) to induce differentiation. qRT-PCR was used to quantify the amount of IVL transcripts relative to cyclophilin A (PPIA) transcripts. Data are the averages and standard errors of the means of two independent experiments. U, uninfected cells; V, vector control; EBV+, EBV-positive clone; EBV-cl 1, 3, and 4, three EBV-negative transiently infected clones.

gene expression readily detected EBER, Qp-initiated EBNA1, LMP2, and the BamHI A rightward transcripts (BARTs). EBNA2 and LMP1 mRNAs were at low levels and were detected only after Southern hybridization with radiolabeled oligonucleotide probes. Quantitative reverse-transcription PCR (qRT-PCR) confirmed low EBNA2 and LMP1 mRNA levels (data not shown). The EBNA1 spliced transcript associated with type III latency (Y3UK) was not detected in the EBV-positive NOK cell lines. Immunofluorescence analysis confirmed the presence of EBNA1 protein in EBV-infected NOK cells (Fig. 2B). Based on Qp-initiated EBNA1 and LMP2 mRNA expression, these results suggested a type I/II latency viral gene expression program in the EBV-positive NOK cell line, similar to the latency state of EBV in gastric carcinoma (37).

Since epithelial cells are sites for EBV lytic replication, we also examined lytic gene expression. Expression of the immediate-early gene transactivator, BRLF1, the early anti-apoptotic gene, BHRF1, and the late glycoprotein gene, gB, was detected at a level similar to B958, which undergoes a low level of spontaneous reactivation. BZLF1 mRNA was not detected by RT-PCR (data not shown). To determine if the lytic gene expression program led to viral replication, the presence of replicative linear forms of EBV DNA were examined in BamHI-digested genomic DNA probed with a radiolabeled NJhet fragment containing the EBV terminal repeats (TRs). Southern blot analysis showed the presence of an abundant fused fragment approximately 10 kb in size representing circular episomes with five to six TRs. A weak, but detectable, lower-molecular-weight band of 6 kb was seen in the size range for linear DNAs, similar to that noted in B958 (Fig. 2C). However, the typical 500-bp laddering was not evident. In addition, gB protein was not detected by Western blotting or immunofluorescence analysis (data not shown). Thus, the infected NOK appeared to harbor a predominantly latent EBV infection with intermittent reactivation either occurring in a few cells or resulting in abortive lytic replication. Similar latent states for epithelial cells have been previously reported following *ex vivo* infection of tonsillar keratinocytes (38, 39). Furthermore, the hTERT-immortalized NOK cell line may be similar to dysplastic epithelia, bridging the gap between normal epithelial cells and carcinoma to favor a latent infection.

To determine if EBV infection interfered with cell growth, we examined cellular proliferation using an MTT [3-(4,5-dimethylthiazol-2-yl)2 2,5-diphenyl tetrazolium bromide] colorimetric-based assay in 24-h intervals up to 96 h. As shown in Fig. 2D, similar growth rates were noted in the 48- to 72-h interval for all cell clones (the EBV-positive, uninfected, vector, and three EBV-

negative transiently infected clones). By 96 h, a slight drop in growth rate in the EBV-positive clone was noted, with a similar decline in the EBV-negative transiently infected clone 4, suggesting that the slight change in growth was independent of EBV. Overall, we concluded that the growth rates of all clones were similar.

Expression of several viral genes (BHRF1, a viral BCL2 homolog, and the viral LMP1 and -2) has been described to inhibit epithelial cell differentiation (40–42). With expression of these viral transcripts in the EBV-positive NOK cells, we questioned if NOK differentiation was hindered in an epigenetic manner following EBV infection. Treatment with calcium chloride induces keratinocyte differentiation and tight junction formation, which can be measured by the ability to form a protective cell barrier and establish a polarized cell layer (43, 44). Transepithelial electrical resistance (TEER) measurements are used as indicators of the permeability of cell layers and are measured by the increased electrical resistance values as cells differentiate. Equal cell numbers were plated in Transwell chambers. When cells reached confluence, calcium chloride was added to stimulate differentiation. TEER was monitored daily for up to 9 days (Fig. 2E). Indeed, the EBV-positive NOK cell line showed lower TEER values starting at day 4 than the uninfected controls. Importantly, the three EBV-negative transiently infected clones were similarly delayed, as noted for the EBV-positive clone, with statistically significant measurements throughout days 4 to 9. Keratinocyte differentiation can also be induced by suspension of cells in methylcellulose (45). Indeed, we observed that uninfected cells induced involucrin transcript levels following a 24-h suspension in methylcellulose compared to cells grown in a monolayer (Fig. 2F). In comparison, the methylcellulose-treated EBV-positive cells and an EBV-negative transiently infected clone showed a reduced and less robust induction of involucrin transcripts (Fig. 2F). These observations suggested that EBV infection of keratinocytes hindered their differentiation potential through epigenetic means, based on retention of the phenotype in clones that had lost EBV.

Global DNA methylation changes following EBV infection of immortalized oral keratinocytes. To investigate epigenetic marks that result in the NOK cell line following EBV infection, we chose to map genome-wide alterations in DNA methylation. We focused on CpG methylation because the distribution of CpG methylation is altered in various EBV-associated malignancies (9, 15–21). EBV immortalization of B cells has been shown to be associated with large-scale hypomethylation that affected two-thirds of the B cell genome and led to promoter hypomethylation of a number of proliferative genes, consistent with the conversion of resting B cells to proliferating blasts (26, 27). In contrast, EBV-associated gastric and nasopharyngeal carcinomas display hypermethylation at a number of tumor suppressor gene promoters (17–20). Since EBV infection has contrasting DNA methylation effects depending on the cellular background, we examined the impact of EBV infection on the cellular methylome of the various NOK cell lines that possibly recapitulated the DNA methylation alterations seen *in vivo*.

Reduced representation bisulfite sequencing (RRBS) was used to map the CpG methylation state on a global scale. For each sample, we obtained approximately 20 to 21 million total reads. Ten to 12 million CpGs aligned to the human genome, mapping 7 to 8 million unique CpG dinucleotides with 7- to 8-fold coverage. The genomic distribution of the mapped CpG residues was similar between the uninfected clone, vector control, EBV-positive clones, and EBV-negative transiently infected clones (Fig. 3A). In the EBV-negative transiently infected clone 1 (cl1), the distribution of mapped CpGs was shifted, with a slight loss at intergenic regions and concomitant gains at exon and promoter regions. Overall, the majority of mapped CpGs were located to intergenic regions (60 to 62%), followed by intronic regions (18%). CpGs in promoters and exons comprised approximately 9% of the total mapped CpGs.

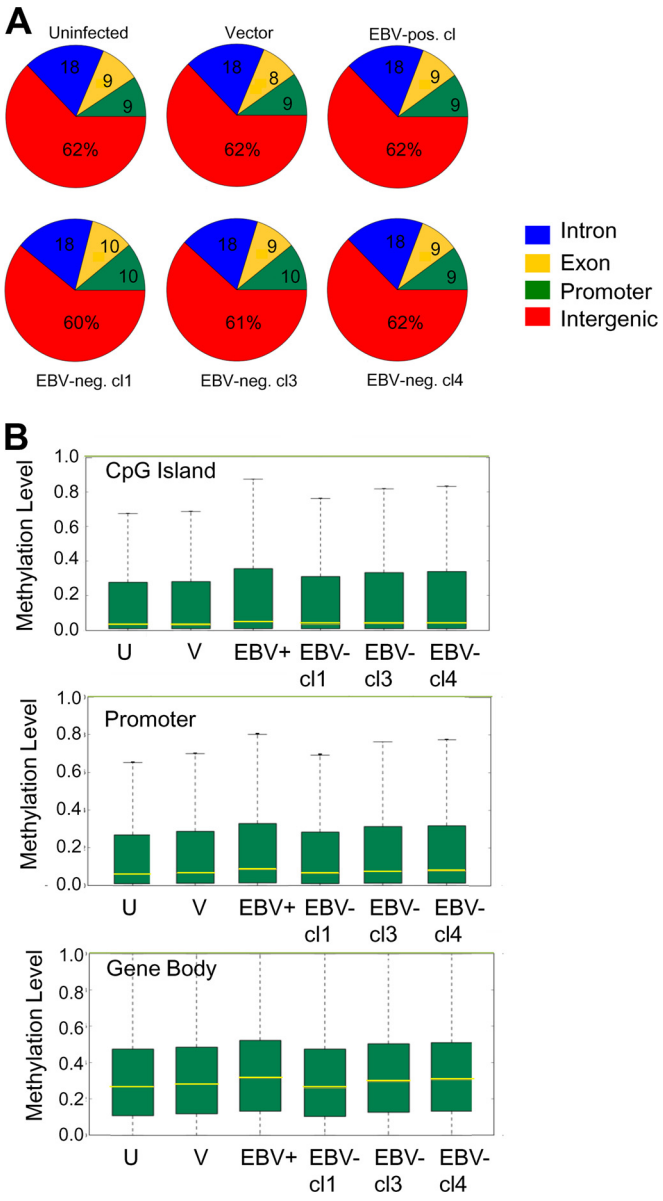

FIG 3 Methylome analysis of NOK by RRBS. (A) Distribution of mapped CpG residues in NOK. (B) Box-and-whisker plots comparing the distribution of methylated CpG residues between uninfected (U) cells, a vector control (V), an EBV-positive clone (EBV+), and three transiently infected EBV-negative clones (EBV-cl1, -cl3, and -cl4) at CpG islands, promoters, and within gene bodies. The yellow line across the bar represents the median level of methylation, the top whisker represents the maximum level of methylation, and the bottom whisker, which goes to 0, represents the minimum level of methylation.

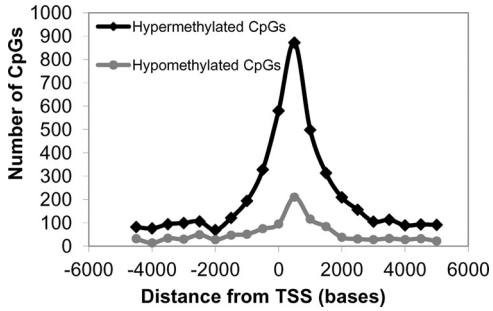

FIG 4 Distribution of differentially methylated CpG residues relative to the transcription start site (TSS). CpGs that either gained methylation (hypermethylated) or lost methylation (hypomethylated) in the EBV-positive and three EBV-negative transiently infected clones in relation to the uninfected and vector control were mapped relative to the TSS.

We next compared the overall methylation level at CpG islands, promoter regions, and within gene bodies between the various methylome samples. As shown in the box-and-whisker plots, the median methylation level of the EBV-positive clone at CpG islands (CGIs), promoter regions, and gene bodies was slightly higher than that observed for the uninfected controls (Fig. 3B). The top 25% of CGIs, promoters, and genes also showed a higher degree of CpG methylation in the EBV-positive clone than the uninfected controls. Similar increases in the levels of DNA methylation at these regions were noted for two EBV-negative transiently infected clones, clones 3 and 4. The DNA methylation levels in EBV-negative transiently infected clone 1 did not appear to be altered relative to the uninfected control.

Although the above results were suggestive of EBV inducing a hypermethylator phenotype in the immortalized keratinocyte cell line, biases from the CpG mapping distribution could influence the methylation frequencies. To overcome this limitation, we identified differentially methylated CpGs that either gained or lost methylation among the various cell clones to compare a common set of CpG residues between the various keratinocyte lines. We identified approximately 13,500 statistically significant differentially methylated CpGs that were common to the EBV-positive and three EBV-negative transiently infected clones relative to the uninfected parental and vector-transfected controls (see Table S2 in the supplemental material). A total of 10,676 CpGs had gained methylation (hypermethylated), while 2,830 CpGs had lost methylation (hypomethylated) in the EBV-positive and transiently infected cells relative to the uninfected controls. These differentially methylated CpG sites did not appear to target specific chromosomes; rather, they were spread across all autosomes and the X chromosome. Since alterations in DNA methylation near transcription start sites (TSS) can influence gene expression, the distance of the differentially methylated CpG residues to the TSS was calculated using the Genomic Position Annotation Tool (GPAT) (46). As shown in Fig. 4 an increase in the frequency of differentially hypermethylated and hypomethylated CpGs occurred within 2 kb upstream and downstream from the TSS, a region with the potential to regulate gene expression.

Promoter hypermethylation as an epigenetic consequence of EBV infection of keratinocytes. Although alteration of the methylation state of individual CpG sites can influence DNA binding factors, alterations of clustered CpGs are better predictors of transcriptional effects. Such clustered CpGs are observed in EBV-associated promoter hypermethylation of silenced tumor suppressor genes in gastric carcinoma or as hypomethylated blocks during EBV B cell immortalization (9, 15–21, 26, 27). To identify such differentially methylated regions (DMR), a sliding-window approach was used to measure the distance between the differentially methylated CpG residues. Those that occurred within 500 bp of each other were counted as belonging to a DMR. Analysis of hypomethylated or hypermethylated DMR showed only 6 genes with loss of five or more methylated CpGs (hypomethylated CpGs) following EBV infection, while 143 genes showed a gain of five or more methylated CpGs following EBV infection (Fig. 5A and B). Hypermethylated DMR with eight or more methylated CpGs occurred on a total of 27 genes, all associated with CGIs. The two genes with the largest number of differentially methylated CpGs were MEIS homeobox protein 1 (MEIS1) and cytoglobin (CYGB), acquiring 32 and 24 methylated CpGs, respectively, on a CGI (see Fig. 9A and B and Table S4 in the supplemental material). Additional examples of CGI methylation included N4BP2L1 and RARRES1, each with 18 and 16 differentially methylated CpGs, respectively (Fig. 5C and D). RARRES1 is observed to be silenced by CGI methylation in nasopharyngeal carcinoma (47). Thus, these data demonstrate that *in vitro* EBV infection of immortalized oral keratinocytes induced a CpG island methylator phenotype (CIMP) similar to what has been observed in EBV-associated carcinomas.

DNA methylation of the EBV genome in EBV-infected keratinocytes. Sequencing reads in the EBV-positive clone were aligned to the Akata EBV strain (KC207813) (35) to map the methylation level of CpG residues of the viral episome in infected keratinocytes. CpG methylation reads from the plus or minus EBV DNA strand with 0 to 20% methylation were classified as unmethylated, while those with 50% to 100% methylation were classified as methylated (see Table S3 in the supplemental material). A limitation of the RRBS approach is poor mapping of repeated genomic regions, which tend to be filtered out in the alignment and are noted by the absence of mapped CpG residues at internal repeat 1 (IR1), IR4, and the terminal repeat regions of the virus. In total, the RRBS approach mapped 3,772 unmethylated CpGs and 1,465 methylated CpGs on the EBV genome (Fig. 6). A hypomethylated state for Akata EBV in NOK was previously reported where various lytic gene promoters were unmethylated (48). Similarly, we observed that all mapped CpGs in the 1 kb region upstream of the transcription start site containing the BZLF1 promoter (Zp) and BRLF1 promoter (Rp) were unmethylated, with 17 and 27 unmethylated CpGs, respectively (see Table S3). The hypomethylated state of Rp was consistent with expression of BRLF1 mRNA. CpG methylation in our EBV-infected NOK occurred sporadically throughout most of the viral genome. However, specific regions of the EBV genome displayed a high density of methylated CpGs residues. These occurred primarily at the BNRF1 gene, flanking the Q exon, the BamHI V fragment, and the BamHI A fragment encoding most of EBV's noncoding RNAs (BARTs) and BALF genes. RT-PCR detected the BART exon 1 transcripts in the EBV-positive NOK cells (Fig. 2A) and appeared not to be silenced by the dense DNA methylation in this region. How these methylated regions influence EBV gene expression is currently unknown, but detection of DNA methylation on the EBV genome provided evidence for viral induction and manipulation of the host DNMTs that likely altered the host methylome as well.

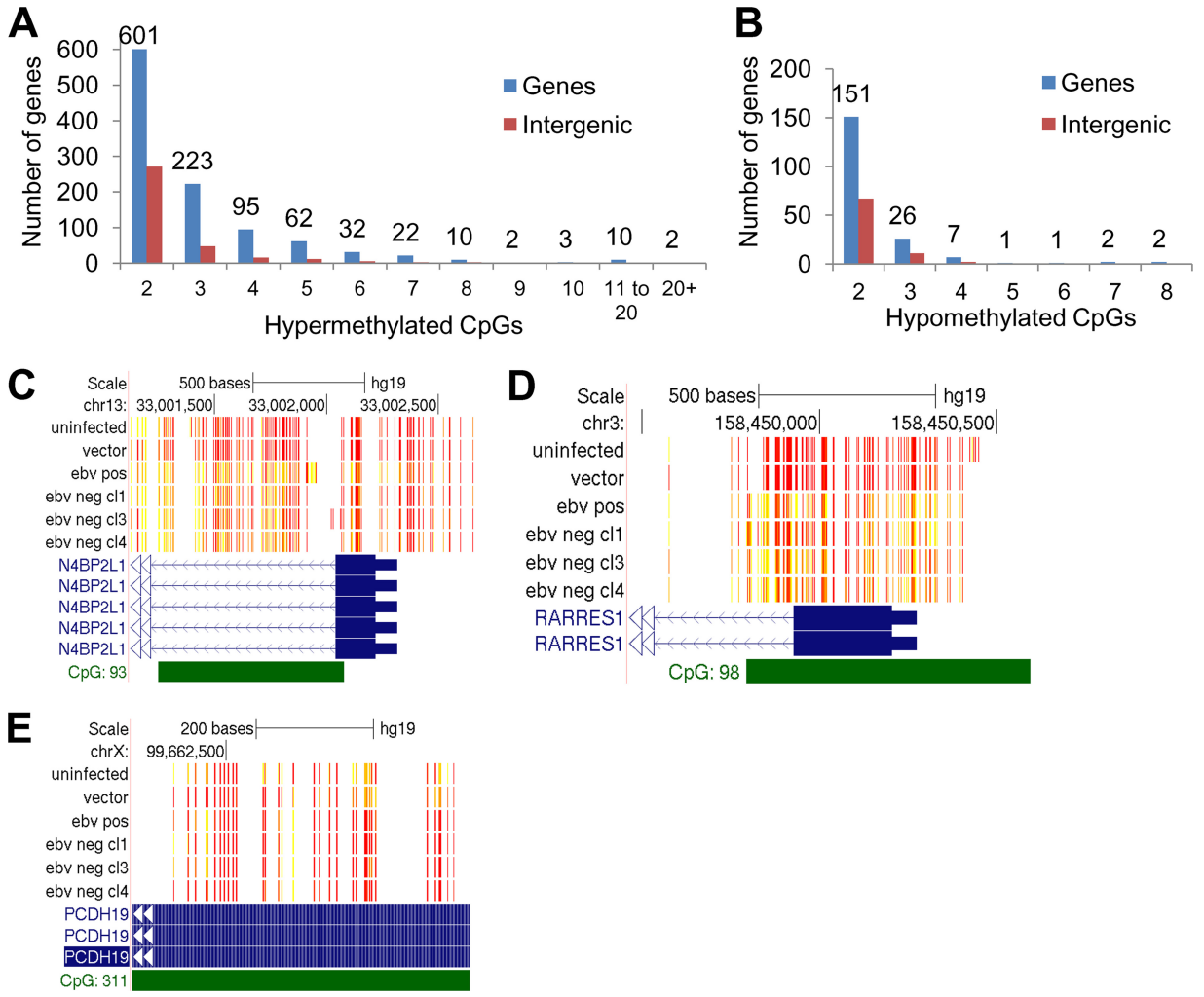

FIG 5 CpG island hypermethylation as an epigenetic consequence of EBV infection of oral keratinocytes. (A) Number of hypermethylation events per locus. (B) Number of hypomethylation events per locus. Differentially methylated CpG residues that were located 500 bases from the previous CpG methylation event were counted. Blue bars indicate the number genes that acquired a certain number of methylation events, while red bars indicate CpG methylation at intergenic locations. (C to E) Methylation tracks at CpG islands in the NEDD4 binding protein 2-like 1 (N4BP2L1) gene, retinoic acid receptor responder 1 (RARRES1) gene, and protocadherin 19 (PCDH19) gene, respectively. Red bars represent unmethylated CpGs, and yellow bars represent methylated CpGs. Solid blue bars represent exons, and green bars represent CpG islands. Direction of transcription is indicated with blue or white arrows. Methylation tracks were visualized using the UCSC (University of California, Santa Cruz) Genome Browser. Samples shown are the uninfected parental control, vector control, an EBV-positive clone (EBV pos), and three EBV-negative transiently infected clones (EBV neg cl1, cl3, and cl4). hg19, human genome build 19.

Epigenetic reprogramming of host gene expression following EBV infection of immortalized oral keratinocytes. By using EBV-negative transiently infected clones, we have observed epigenetic alterations following EBV infection at the level of DNA methylation and functionally through reduced keratinocyte polarization and barrier formation. To determine if the EBV-induced epigenetic changes were correlated with altered host gene expression, Affymetrix U133 Plus 2.0 microarrays were used to measure RNA levels of duplicate biological replicates: an uninfected, vector-transfected, and EBV-positive clone and three transiently infected clones. First, we compared the transcriptional profiles of the samples using principal component analysis (PCA), a statistical analysis technique that reduces the complexity of large data sets into its principal components which retain most of the variability present in the original values (49). PCA is an orthonormal transformation which projects data from some matrix D onto a new coordinate system, where D is usually mean centered and normalized. Principal components are comparable to a rigid body's principal axes and are linearly uncorrelated variables (50). PCA results in an ordered set of loading vectors w such that (when applied in the dot product of itself and each data vector) the first principal component has the greatest possible variance; subsequent components have maximal variance when they are uncorrelated with previous components. Through PCA, the relatedness (variability and similarities) of samples can be determined, and we exploited this approach to compare the variances in gene expression between our samples.

A reduced data set of ~5,500 genes was used that focused on statistically significant ($P < 0.05$) gene expression changes between any of the cell samples as determined by ANOVA. Reduction removed the nonsignificant background gene changes yet retained the variability among the samples to enhance sample dis-

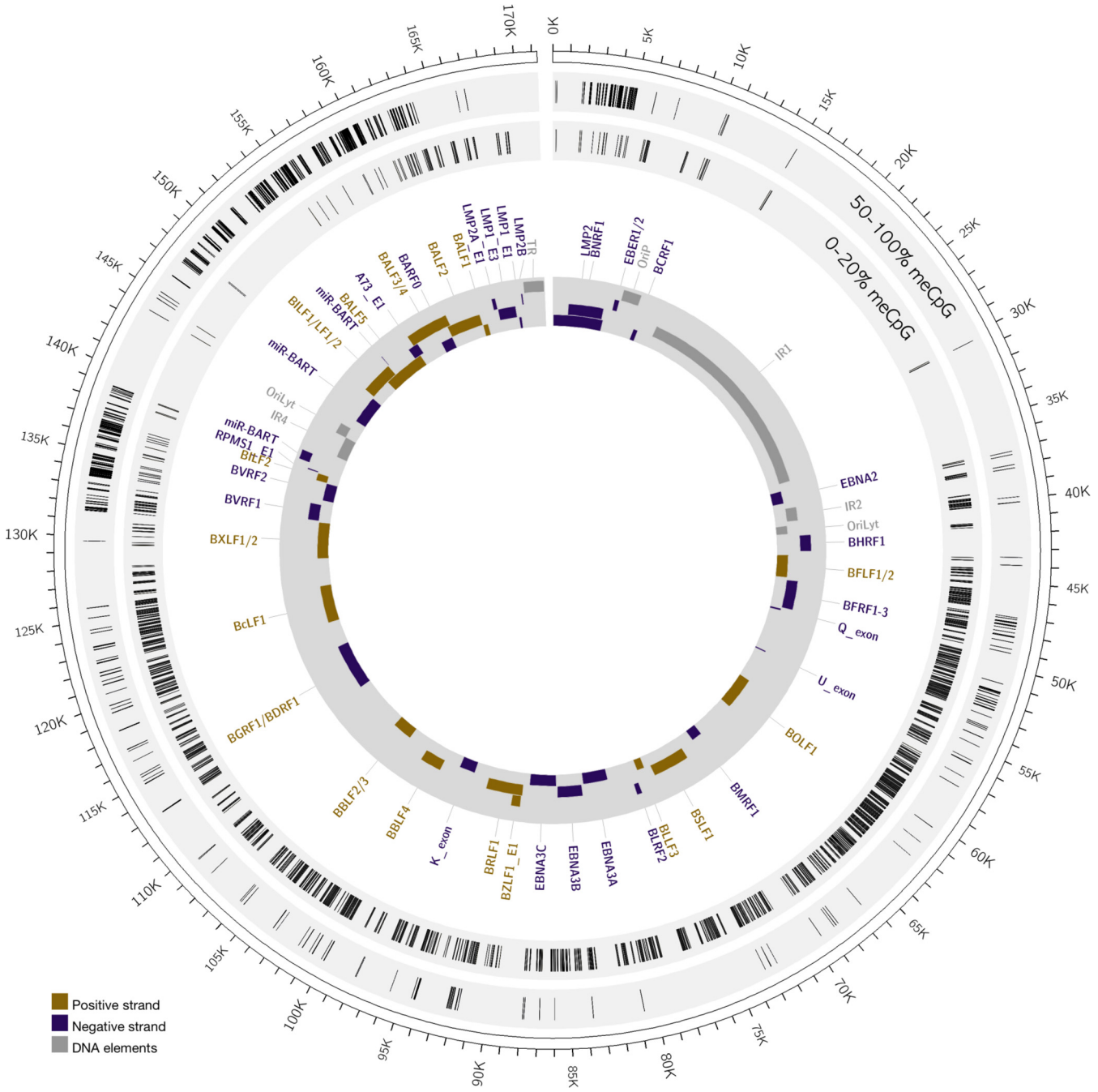

FIG 6 Methylation of the EBV genome in stably infected NOK. The outer circle displays the EBV genome position. The inner gray circle annotates select EBV genes, with purple bars showing rightward reading open reading frames and gold bars indicating the leftward reading open reading frames. Repetitive elements and origins of DNA replication are indicated as gray bars. The light gray circles map the positions of methylated (50 to 100% meCpG) and unmethylated (0 to 20% meCpG) CpG residues.

crimination in PCA. As expected, PCA showed a close relationship between the uninfected parental clone and vector-transfected clone, which clustered closely together (Fig. 7A and B). The EBV-positive clone was the most distant from the EBV-negative cells and was likely a result of viral gene expression known to alter host gene expression. Intriguingly, the three EBV-negative transiently infected clones clustered together, being most similar to each other, but were still separated from the uninfected controls. These results suggested that the transcriptional profiles were epigenetically regulated following EBV infection since loss of the viral episome did not completely restore the transcriptional profile to that of the uninfected controls.

To identify differentially expressed genes as a result of EBV epigenetic manipulation, we performed a pairwise comparison between expression data sets from the group of cells exposed to EBV (EBV-positive and three EBV-negative transiently infected

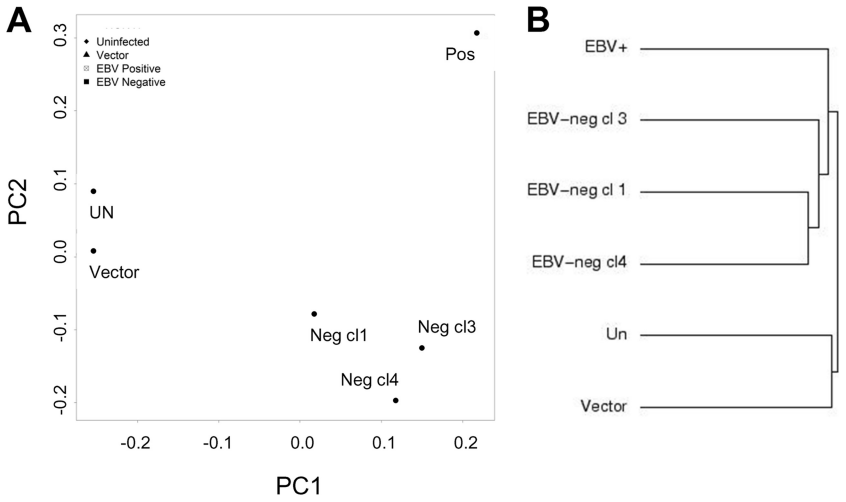

FIG 7 Altered gene expression patterns as a consequence of EBV-induced epigenetic alterations. (A) Principle component analysis (PCA) of gene expression using a subset of 5,500 genes of uninfected (UN) cells, a vector control (vector), an EBV-positive clone (Pos), and three EBV-negative transiently infected clones (Neg cl1, -cl3, and -cl4). (B) Dendrogram based on PCA showing clustering of samples according to EBV exposure.

clones) and to uninfected controls (uninfected parental and transfected vector control). Such an approach would increase the statistical power and focus on a common set of gene expression changes following EBV infection and reduce contributions from clonal variation. A total of 357 probe set identifiers (IDs) were found to be differentially expressed, constituting 260 unique and annotated differentially expressed genes; 139 genes were downregulated, and 121 genes were upregulated in cells exposed to EBV relative to uninfected controls (see Table S5 in the supplemental material). Ontological classification of genes using Ingenuity Pathway Analysis revealed gene associations with cancer (128 genes, $P < 0.015$), cell-to-cell signaling interaction (58 genes, $P < 0.015$), and organismal development (47 genes, $P < 0.015$). Further exploration in Ingenuity Pathway Analysis predicted inhibitory effects in the transcriptional networks involving RelA and tumor protein p63 (with Z scores of -2.6 and -2.1, respectively) (see Fig. S1 in the supplemental material). RelA/p65 is a member of the NF-κB family of transcription factors. NF-κB has well-established proinflammatory functions but is also a crucial factor in regulating immune homeostasis and prevention of inflammatory disease in epithelial tissues (51). For RelA, the downstream targets BEX2, CCL20, CXCL1, intercellular adhesion molecule 1 (ICAM-1), interleukin-12A (IL-12A), Toll-like receptor 2 (TLR2), and UGT1A1 were downregulated in cells exposed to EBV relative to uninfected controls. Thus, manipulation of these downstream NF-κB targets following EBV infection suggests a modulation of immune surveillance that might enhance viral persistence in epithelial tissues. The second affected network involved p63, a member of the p53 family of transcription factors crucial in the formation and maintenance of stratified epithelia (52, 53). p63 encodes various isoforms with transcriptional activation and repressive functions. The expression states of upregulated (COL5A1, TNC, and WNT5A) and downregulated (ADAMTS1, BST2, IGFBP7, SPRR3, and ULK2) gene targets predicted an inhibitory state of p63. Intriguingly, the RelA network was also noted to be downstream of p63. The IκB kinase alpha (IKKα) is a downstream target of p63, essential for epithelial differentiation (53), and a kinase that activates NF-κB nuclear translocation (54). EBV LMP2A has also been shown to induce the ΔNp63α isoform which results in impaired epithelial differentiation (55). Thus, these gene associations that predicted an inhibitory state of RelA and p63 were consistent with the delayed calcium- and methylcellulose-induced differentiation of EBV-positive and transiently infected EBV-negative keratinocytes (Fig. 2E and F).

Comparison of the differential gene expression and DNA methylation data identified 65 genes that acquired DNA methylation (Table 1). All genes had evidence of CpG methylation, with only two genes showing both gain and loss of CpG methylation. DNA methylation changes that occurred on differentially expressed genes accounted for a minority of differentially methylated genes, suggesting that the majority of gene expression changes may be downstream of potential key regulatory genes that are methylated. Of methylated genes showing altered expression, 33 were downregulated while 32 were upregulated in cells with prior EBV exposure compared to uninfected controls. Ingenuity Pathway Analysis focusing on the 33 downregulated targets with EBV-induced DNA methylation revealed three methylated targets downstream of RelA (BEX2, CXCL2, and TLR2).

The positioning of DNA methylation in the transcriptional unit can have various outcomes on gene expression. DNA methylation near the transcription start site (TSS) can block transcription initiation (56). DNA methylation in the gene body generally does not impede transcription initiation but can have posttranscriptional effects by influencing RNA splicing in a positive or negative manner (56). Indeed, 25 out of 33 downregulated genes had evidence of DNA methylation within 2 kb from the TSS, consistent with the role of DNA methylation playing a key role in altering gene expression.

In the upregulated genes, CpG methylation within 2 kb from the TSS occurred in 8 out of 32 genes (Fig. 8A). Further analysis showed that the downregulated genes had methylated CpGs at a median distance of 504 bases from the TSS (Fig. 8B). In upregulated genes, CpG methylation was much farther away, occurring at a median distance of 20,700 bases from the TSS (Fig. 8B). In addition, DNA methylation on the downregulated gene set predominantly occurred at CGIs or CGI shores (30/33 downregulated

TABLE 1 Correlation of DNA methylation on differentially expressed genes in transiently infected clones compared to uninfected controls

Gene group and symbol	Gene name or description	Total no. of meCpGs[a]	No. of meCpGs (DMR)	meCpG element	Avg TSS distance (bases)	Fold change in expression[b]	*P* value[b]
Downregulated genes							
CYGB	Cytoglobin	24	24	CGI	385	−1.9	0.027
IGFBP7	Insulin-like growth factor binding protein 7	7	7	CGI	278	−1.9	0.001
HTATIP2	HIV-1 Tat-interactive protein 2, 30 kda	5	5	CGI	433	−5.5	0.001
LINC00461	Long intergenic non-protein coding RNA 461, microRNA 9-2	4	2	CGI	13,050	−4.9	0.005
SETD6	SET domain containing 6	3	3	Shore	724	−31.8	0.0001
PASD1	PAS domain containing 1	3	3	None	655	−7.8	0.003
PCDHB6	Protocadherin beta 6	3	2	Shore	441	−6.7	0.001
HERC5	Hect domain and RLD 5	3	3	CGI	354	−2.0	0.042
TSTD1	Thiosulfate sulfurtransferase (rhodanese)-like domain containing 1	2	2	CGI	182	−50.7	0.001
ZC3HAV1L	Zinc finger CCCH-type, antiviral 1-like	2	2	CGI	23	−10.3	0.02
TLR2	Toll-like receptor 2	2	2	CGI	247	−4.4	0.001
NLGN1	Neuroligin 1	2	2	CGI	713	−3.2	0.022
BEX2	Brain expressed X-linked 2	2	2	CGI	123	−3.3	0.001
NPR2	Natriuretic peptide receptor B/guanylate cyclase B (atrionatriuretic peptide receptor B)	2	2	CGI	504	−2.4	0.007
RNLS	Renalase, FAD-dependent amine oxidase	2	2	CGI	280	−2.1	0.003
SESN3	Sestrin 3	2	2	CGI	1,269	−2.1	0.001
B3GALNT1	Beta-1,3-*N*-acetylgalactosaminyltransferase 1 (globoside blood group)	2	0	CGI	389	−6.3	0.001
PCDH10	Protocadherin 10	2	0	CGI	2,305	−4.3	0.001
SYK	Spleen tyrosine kinase	2	0	None	38,241	−2.3	0.001
FAM129B	Family with sequence similarity 129, member B	2	0	Shore	61,403	−1.9	0.006
GPR158	Signal transduction, G-protein-coupled receptor signaling pathway	1	0	CGI	1,346	−22.6	0.02
BCAT1	Branched chain amino acid transaminase 1, cytosolic	1	0	CGI	824	−5.4	0.001
CCDC88C	Coiled-coil domain containing 88C	1	0	CGI	364	−2.9	0.002
NEFL	Neurofilament, light polypeptide	1	0	CGI	63	−2.8	0.003
HRASLS	HRAS-like suppressor	1	0	CGI	195	−2.7	0.038
DUOX1	Dual oxidase 1	1	0	CGI	391	−2.7	0.003
CXCL1	Chemokine (C-X-C motif) ligand 1 (melanoma growth stimulating activity, alpha)	1	0	Shore	534	−2.3	0.002
THOC5	THO complex 5	1	0	Shore	1,042	−2.1	0.013
MEST	Mesoderm-specific transcript homolog (mouse)	1	0	CGI	5,220	−2.0	0.033
ERVMER34-1	Endogenous retrovirus group MER34, member 1	1	0	CGI	408	−1.9	0.009
SLC12A8	Solute carrier family 12 (potassium/chloride transporters), member 8	1	0	Shore	69,933	−1.9	0.03
ATP5J2-PTCD1	ATP5J2-PTCD1 readthrough, pentatricopeptide repeat domain 1	1	0	None	8,656	−1.9	0.004
MMRN2	Multimerin 2	1	0	CGI	14,572	−1.8	0.011
Upregulated genes							
FBXL16	F-box and leucine-rich repeat protein 16	20	7	CGI	9,233	3.8	0.001
FAM20C	Family with sequence similarity 20, member C	13	5	Shore	90,178	4.6	0.001
COL5A1	Collagen, type V, alpha 1	12	3	None	83,290	2.8	0.001
ZIC2	Zic family member 2	8	6	CGI	682	10.7	0.013
HS6ST2	Heparan sulfate 6-*O*-sulfotransferase 2	8	7	CGI	3,971	1.9	0.021
TBX3	T-box 3	7	5	CGI	9,751	2.2	0.002
EPHB2	EPH receptor B2	7	3	None	92,791	2.0	0.011
AUTS2	Autism susceptibility candidate	7	3	None	1,148,930	2.9	0.001
SOBP	*Sine oculis* binding protein homolog (*Drosophila*)	6	6	CGI	145,077	6.7	0.009
AGPAT3	1-Acylglycerol-3-phosphate *O*-acyltransferase 3	6	4	None	65,817	2.6	0.005
PLXND1	plexin D1	5	5	CGI	764	2.5	0.005
APBA2	Amyloid beta (A4) precursor protein-binding, family A, member 2	5	3	CGI	158,788	2.4	0.019
LEF1	Lymphoid enhancer-binding factor 1	4	2	CGI	12,844	67.6	0.001
KCNH5	Potassium voltage-gated channel, subfamily H (Eag-related), member 5	4	2	CGI	37,186	1.9	0.001
LINGO2	Leucine-rich repeat and Ig domain containing 2	3	2	None	167,376	1.95	0.033
CYB561	Cytochrome *b*-561	3	0	CGI	1,947	1.9	0.006
WNT5A	Wingless-type MMTV integration site family, member 5A	2	2	CGI	6,898	46	0.001
LINC00478	Long intergenic non-protein coding RNA 478	2	2	None	315,730	1.8	0.03
DOHH	Deoxyhypusine hydroxylase/monooxygenase	2	2	None	10,309	1.81	0.011
ADAMTS20	ADAM metallopeptidase with thrombospondin type 1 motif, 20	2	0	CGI	509	4.0	0.001
CXADR	Coxsackie virus and adenovirus receptor	1	0	None	25,235	3.8	0.015
SYTL4	Synaptotagmin-like 4	1	0	None	7,861	3.4	0.001
HHIP	Hedgehog interacting protein	1	0	Shore	985	3.4	
RRAGD	Ras-related GTP binding D	1	0	CGI	191	3.0	0.047
METTL20	Methyltransferase-like 20	1	0	None	1,471	2.4	0.048
LOC440173	Uncharacterized LOC440173	1	0	CGI	30,454	2.3	0.006
LOC283683/LOC646278	Uncharacterized LOC283683, programmed cell death 6 interacting protein pseudogene	1	0	None	52,565	2.3	0.003
IL21R	Interleukin-21 receptor	1	0	None	16,158	2.1	0.038
TRIML2	Tripartite motif family-like 2	1	0	CGI	1,280	1.9	0.04

(Continued on following page)

TABLE 1 (Continued)

Gene group and symbol	Gene name or description	Total no. of meCpGs[a]	No. of meCpGs (DMR)	meCpG element	Avg TSS distance (bases)	Fold change in expression[b]	*P* value[b]
ABCA1	ATP-binding cassette, subfamily A (ABC1), member 1	1	0	None	112,091	1.9	0.003
MYO5B	Myosin VB	1	0	None	255,686	1.8	0.002
CSMD1	CUB and Sushi multiple domains 1	1	0	None	1,892,786	1.8	0.041

[a] meCpG, methylated CpG.
[b] Change in expression relative to uninfected controls.

genes) (Table 1). CGI shores are the 2-kb regions flanking the CGIs and are also frequently targeted for DNA methylation (57). In the upregulated gene set, half of the genes (17/32 genes) (Table 1) demonstrated CGI methylation, but the majority of these methylated CGIs (10/17 methylated CGIs in upregulated genes) were located far from the TSS and within the gene body.

To determine if repression of gene expression was due to the acquisition of methylated CpGs noted for a number of genes, cells were treated with the DNMT inhibitor decitabine (DAC), and RNA levels were measured by qRT-PCR. Candidate hypermethylated genes included those that were shown by the microarray experiment to be repressed (CYGB, HIV Tat-interactive protein 2 [HTATIP2], protocadherin beta 6 [PCDHB6], and PAS domain containing 1 [PASD1]). We also included MEIS1, the top hypermethylated gene with 32 methylated CpG residues, to determine through a more sensitive technique if CGI hypermethylation affected MEIS1 mRNA levels that were potentially missed by the microarray analysis. MEIS1 is a developmental gene whose overexpression is associated with the initiation and maintenance of mixed-lineage leukemia (MLL) protein-associated leukemias. Loss of MEIS1 expression has been observed in prostate and colon carcinomas, with evidence of it being hypermethylated in BRAF mutated colon cancers (58). qRT-PCR showed that MEIS1 mRNA levels did not change (similar to what we observed in the microarray experiment) despite the CGI hypermethylation noted in cells infected with EBV relative to uninfected controls (Fig. 9A). DAC treatment increased MEIS1 mRNA levels in all samples except for the EBV-positive clone, indicating some role, although not specific to the EBV-induced hypermethylation event, for DNA methylation in regulating MEIS1 expression.

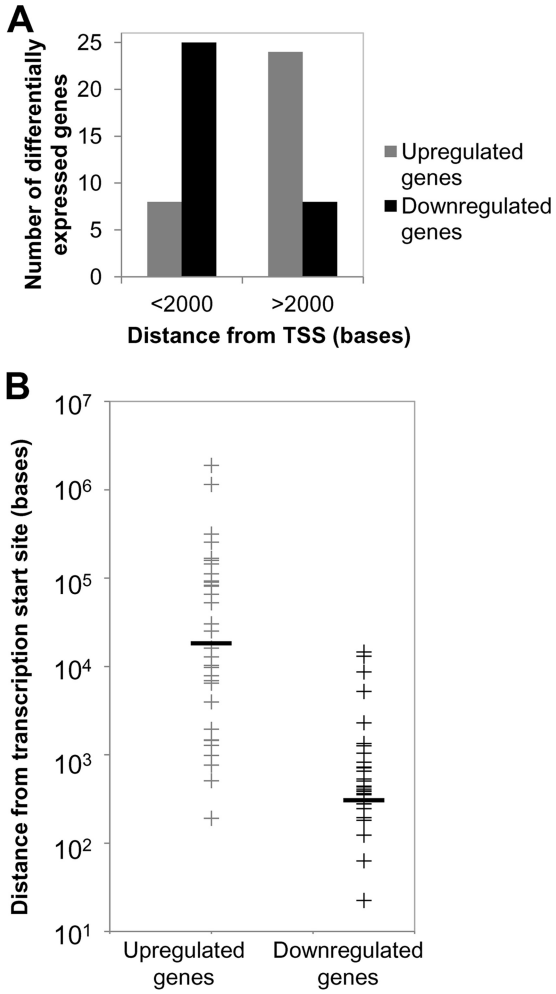

FIG 8 Positional effect of DNA methylation on gene expression. (A) Differentially expressed genes were grouped according to whether the position of DNA methylation was near the TSS (<2,000 kb) or far from the TSS (>2,000 kb). (B) Distribution of methylation from the transcription start site (TSS) on differentially expressed genes (upregulated or downregulated) in an EBV-positive clone and the three EBV-negative transiently infected clones compared to uninfected cells and vector controls. Black horizontal bars indicated the mean distances of methylation from the TSS.

We next analyzed a subset of repressed genes that had evidence of CpG methylation following EBV infection. CYGB was the second most hypermethylated gene on our list, with 24 methylated CpG residues. CYGB is ubiquitously expressed and is thought to protect against oxidative stress. Downregulation of CYGB has been observed in many human malignancies (59). qRT-PCR analysis confirmed an approximate 2-fold reduction in mRNA levels in cells exposed to EBV compared to uninfected controls (Fig. 9B). DAC treatment restored CYGB to similar levels between the samples, suggesting that the 2-fold reduction in mRNA levels following EBV infection was related to the CGI hypermethylation observed. HTATIP2, a tumor suppressor oxidoreductase that acquired five hypermethylated CpG residues following EBV infection, was silenced in the EBV-positive clone and two EBV-negative transiently infected clones (Fig. 9C). HTATIP2 mRNA levels in the EBV-negative, transiently infected clone 1 were not reduced and were similar to the mRNA levels of uninfected cells and the vector control. This particular clone did not demonstrate high methylation levels, as shown in Fig. 2B, and also indicated some heterogeneity in the epigenetic events following EBV infection. DAC treatment partially increased HTATIP2 mRNA levels but did not reach the mRNA levels of the treated uninfected controls. This observation suggested that other factors such as chromatin modifications in the transcriptional silencing of HTATIP2.

Not all CpG methylation occurred at CGIs. At PCDHB6, differential CpG methylation occurred at a CGI shore, while PASD1

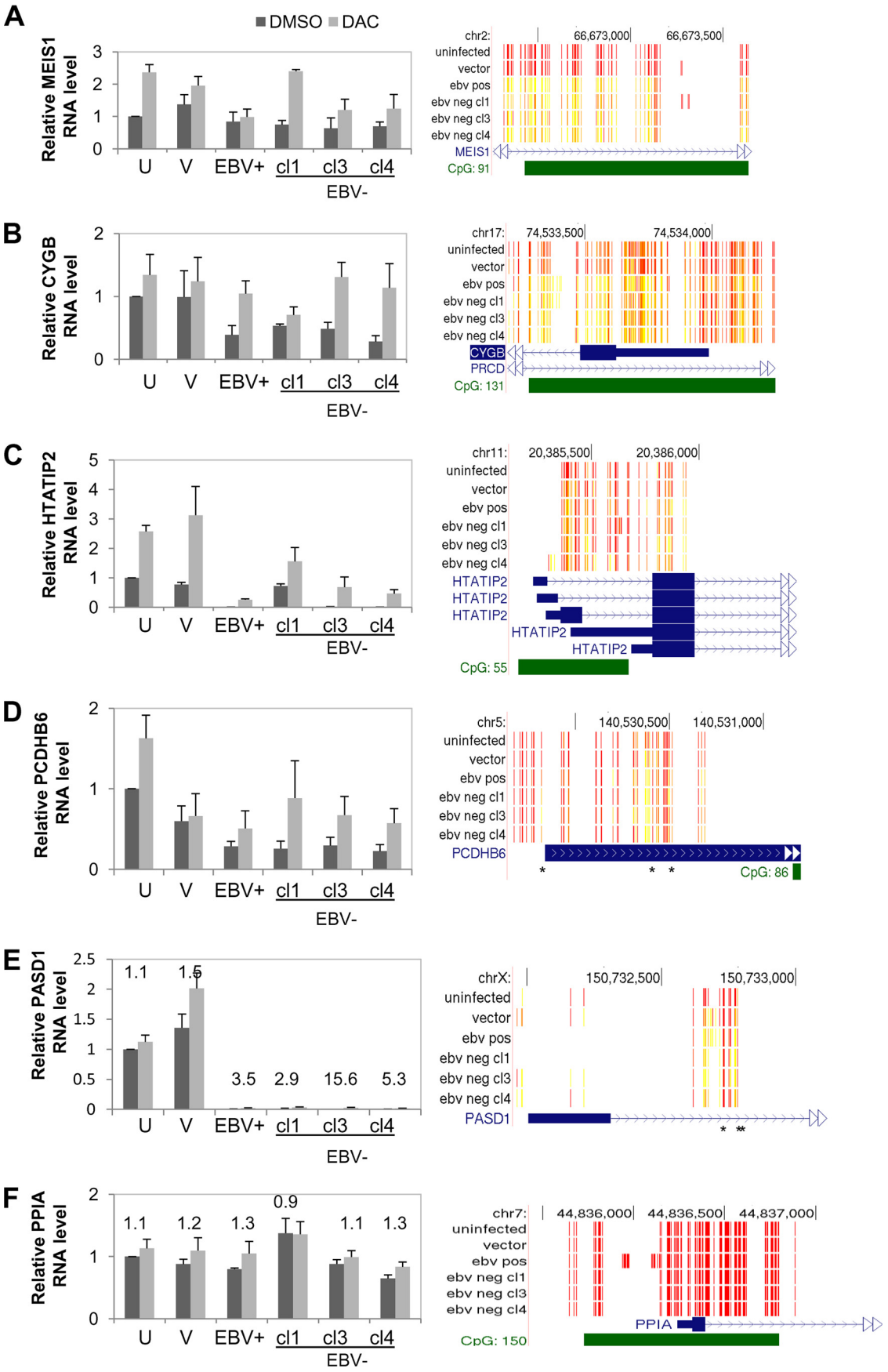
A
DMSO DAC
Relative MEIS1 RNA level
3
2
1
0
U V EBV+ cl1 cl3 cl4
EBV-
chr2: 66,673,000 66,673,500
uninfected
vector
ebv pos
ebv neg cl1
ebv neg cl3
ebv neg cl4
MEIS1
CpG: 91
B
Relative CYGB RNA level
2
1
0
U V EBV+ cl1 cl3 cl4
EBV-
chr17: 74,533,500 74,534,000
uninfected
vector
ebv pos
ebv neg cl1
ebv neg cl3
ebv neg cl4
CYGB
PRCD
CpG: 131
C
Relative HTATIP2 RNA level
5
4
3
2
1
0
U V EBV+ cl1 cl3 cl4
EBV-
chr11: 20,385,500 20,386,000
uninfected
vector
ebv pos
ebv neg cl1
ebv neg cl3
ebv neg cl4
HTATIP2
HTATIP2
HTATIP2
HTATIP2
HTATIP2
CpG: 55
D
Relative PCDHB6 RNA level
2
1
0
U V EBV+ cl1 cl3 cl4
EBV-
chr5: 140,530,500 140,531,000
uninfected
vector
ebv pos
ebv neg cl1
ebv neg cl3
ebv neg cl4
PCDHB6
CpG: 86
E
Relative PASD1 RNA level
2.5
2
1.5
1
0.5
0
1.1 1.5 3.5 2.9 15.6 5.3
U V EBV+ cl1 cl3 cl4
EBV-
chrX: 150,732,500 150,733,000
uninfected
vector
ebv pos
ebv neg cl1
ebv neg cl3
ebv neg cl4
PASD1
F
Relative PPIA RNA level
2
1
0
1.1 1.2 1.3 0.9 1.1 1.3
U V EBV+ cl1 cl3 cl4
EBV-
chr7: 44,836,000 44,836,500 44,837,000
uninfected
vector
ebv pos
ebv neg cl1
ebv neg cl3
ebv neg cl4
PPIA
CpG: 150

showed a gain of three methylated intronic CpGs and loss of two methylated CpGs occurring in the promoter region. PCDHB6 is a member of the cadherin family involved in homotypic cell-to-cell connections. Analysis of PCDHB6 mRNA levels following DAC treatment restored the mRNA levels in the EBV-positive and transiently infected clones to the levels observed in the treated uninfected cells (Fig. 9D). On the other hand, the silencing of PASD1 mRNA levels, a cancer testes antigen with potential transcription factor activity, could not be restored to uninfected levels by DAC treatment and again implicated epigenetic regulation by chromatin and other unknown factors (Fig. 9E). Finally, we ensured that the observed mRNA levels were not due to altered expression of the housekeeping control gene, HPRT, in the various clones or after DAC treatment. HPRT mRNA levels were compared to those of a second housekeeping gene control (cyclophilin A, PPIA). As expected, PPIA mRNA normalized to HPRT mRNA was similar among all clones with or without DAC treatment, validating the qRT-PCR analysis (Fig. 9F). In sum, restoration of mRNA levels following DAC treatment of CYGB, HTATIP2, and PCDHB6 demonstrated that DNA methylation changes following EBV infection can have lasting consequences on gene expression that persist long after loss of the virus. In other cases (HTATIP2 and PASD1), DAC treatment did not reverse or partially reversed the epigenetic repression of gene expression, implicating other epigenetic factors in maintaining the gene expression state.

DISCUSSION

In this study, we examined the epigenetic consequences of EBV infection in an immortalized oral keratinocyte cell line, NOK. We utilized a transient EBV infection cell system to identify "true" epigenetic changes that occur following infection. As epigenetic alterations are defined as being heritable, this approach has helped us identify epigenetic changes that were not dependent on continued viral gene expression and could persist in latently infected carcinoma. A clonal NOK cell line was used for infection to avoid epigenetic alterations that could potentially result from clonal selection and also provide a uniform epigenetic state as a reference. In the transiently infected, EBV-negative clones derived from EBV-infected NOK, we observed that EBV-induced epigenetic alterations influenced the differentiation state, the DNA methylation state that included a CGI hypermethylator phenotype at a number of gene loci, and gene expression states, all being epigenetically inherited over many cell generations and propagated in the absence of viral gene expression.

EBV infection of epithelial cells *in vitro* typically is inefficient, and the viral genome is rapidly lost. To overcome these limitations, selection pressure needed to be applied to maintain the viral episome. In stably infected NOK cells, we observed a predominant latent gene expression pattern with a small subset of cells expressing late lytic transcripts as an indicator of viral reactivation or abortive lytic replication. However, we cannot exclude the possibility that the latent viral state of the infected NOK was selected for in our approach. Although epithelial cells are considered sites of lytic/productive EBV infection, EBV-associated carcinoma cells tend to display a latent EBV infection with silencing by of the EBV immediate-early genes, BZLF1 and BRLF1, by DNA methylation (60). However, the stably infected NOK lacked DNA methylation at the Zp and Rp promoter regions, similar to the hypomethylated state of various lytic promoter regions previously reported in EBV-infected NOK (48). Lytic replication and viral reactivation of such hypomethylated genomes can be induced by BRLF1 rather than BZLF1 (48), an expression pattern noted in our EBV-infected NOK (Fig. 2A and B). Together, the ability of EBV to establish a latent infection in the NOK cells may reflect the immortalized state of these cells or be a transient latency compartment, with spontaneous reactivation occurring to maintain viral persistence. Importantly, EBV infection of NOK epigenetically impaired keratinocyte differentiation as EBV-negative transiently infected clones were similarly refractory to calcium and methylcellulose induction of differentiation (Fig. 2E and F). Although several EBV latent proteins are known to inhibit epithelial differentiation, here we show that viral infection has long-term epigenetic effects to retain a basal cell phenotype.

Using RRBS, we were able to map the methylation state of over 5,000 CpG residues on the EBV genome. Mapping of the DNA methylation state was not complete, as noted at repetitive regions of the genome, due to limitations of RRBS. Although EBV genomes appeared to be predominantly latent, evidence for lytic replication was noted (Fig. 2A) that could skew the methylation profiles of the EBV genome but likely reflect the state of the EBV genome in the epithelium. We observed that mapped CpG residues from the EBV genome showed a propensity for being hypomethylated (3,772 unmethylated CpGs versus 1,465 methylated CpGs) (see Table S3 in the supplemental material). Intriguingly, methylated CpG residues were evident throughout the genome, with several regions being densely methylated (Fig. 6). The reason for the dense CpG methylation at specific viral loci remains unclear and likely involves various mechanisms of regulation. For example, dense methylation was observed in the region encoding the BARTs that also produce over 40 viral microRNAs (miRNAs). DNA methylation in this region may potentially regulate splicing of the BamHI A transcripts and, in turn, production of the viral miRNAs or regulate expression of the leftward transcripts. Dense methylation was also noted at the boundaries of Qp, which is typically unmethylated. Moreover, this dense methylation seems to mark repressive chromatin boundaries that have been shown to spread into the unmethylated Qp in the absence of CTCF binding element (13). Evidence of DNA methylation on the viral episome would support EBV manipulation of the host epigenetic machinery to deposit or maintain the DNA methylation state. However, activation of DNMTs or other chromatin modulators in EBV-infected NOK needs further examination.

FIG 9 Correlation of DNA methylation with repression of gene expression using the DNMT inhibitor, DAC. Bar graphs show the relative mRNA expression levels of MEIS homeobox protein 1 (MEIS1), cytoglobin (CYGB), HIV-1 Tat-interactive protein 2 (HTATIP2), protocadherin beta 6 (PCDHB6), PAS domain containing 1 (PASD1), and cyclophilin A (PPIA), respectively. NOK were treated with 1 μM DAC or an equal volume of DMSO as a vehicle control for 96 h. mRNA levels were determined by qRT-PCR and normalized to the level of hHPRT using the standard curve method. The relative RNA levels were determined by arbitrarily setting the uninfected (U), DMSO vehicle control to 1. Data are the averages and standard errors of the means from three independent biological treatments. In panels E and F, fold difference between the DAC-treated and DMSO vehicle control are shown. Right panels display the methylation tracks at regions where differential methylation was observed following EBV infection. These tracks were visualized using the UCSC (University of California, Santa Cruz) Genome Browser. Red bars represent unmethylated CpG residues; yellow bars represent methylated CpG residues.

In contrast to the methylation state of the EBV genome, DNA methylation patterns of the keratinocyte genome following EBV infection showed gains in CpG methylation. Some heterogeneity among EBV-negative transiently infected clones was noted both at the levels of DNA methylation and gene expression, suggesting that EBV likely did not infect cells with preexisting methylation patterns. Rather, we contend that EBV infection induced hypermethylation of a select number of genes that was beneficial to viral persistence. Twenty-seven genes having eight or more methylated CpGs all acquired their methylation events on CGIs and clearly showed a CGI hypermethylated phenotype (Fig. 5). However, only a few of these genes had evidence of being transcriptionally altered. Reasons for the apparent lack of transcriptional effects by DNA methylation include the following: (i) existing DNA methylation at the CGI in question such that newly acquired methylated CpG residues would be redundant with the existing state and (ii) a role for other chromatin modifications and transcription factors in the regulation of gene expression. Chromatin is likely an important mediator in transcriptional regulation, with DNA methylation coming as a second event for gene repression. Genes marked with bivalent histone modifications (histone H3 dimethylated on lysine 4 [H3K4me2] and trimethylated on lysine 27 [H3K27me3]) at CpG islands can gain repressive heterochromatin histone modifications targeting that CpG island for DNA methylation (61). Such a switch in chromatin states would likely not change reduced or silent transcript levels. We should note that the effects of DNA methylation were assayed under optimal growth conditions, unlike what cancer cells or epithelial cells may encounter *in vivo*. Under conditions that induce differentiation, we observed a delayed ability to form a polarized differentiated layer in transiently infected EBV-negative clones relative to the uninfected controls. We speculate that under different stimuli, such as induction of differentiation by calcium chloride or during tumor evolution, the effect of DNA methylation changes would likely show altered transcriptional states for additional hypermethylated genes. Of importance is that *in vitro* EBV infection of oral keratinocytes recapitulated the CGI hypermethylation observed to occur in EBV-associated gastric and nasopharyngeal carcinomas, specifically RARRES1 hypermethylation, which has been reported for nasopharyngeal carcinomas (47).

A subset of differentially methylated genes was identified that correlated the acquired DNA methylation to altered transcript levels following EBV infection. Several of these genes were part of transcriptional networks involving RelA and p63, transcription factors with roles in regulating epithelial differentiation. Differential DNA methylation acquired near the TSS was predictive of repressed genes and was associated with CGIs. These observations are consistent with a promoter-associated CGI being associated with transcriptional repression (56). Loss of DNA methylation using the DNMT inhibitor decitabine restored RNA levels in three of four genes examined and supported the role of DNA methylation in transcription repression (Fig. 9). However, partial responses of some of these genes also suggested other epigenetic effects, i.e., histone modifications or noncoding RNA, occurred in response to EBV infection. Analysis of upregulated genes revealed a different pattern of methylation following EBV infection (Fig. 8). Upregulated genes acquired differential DNA methylation usually within the gene body distant from the TSS. CGI methylation was still apparent in half of the genes but positioned farther from the TSS, which was more predictive of transcriptional induction. How these differentially methylated CpGs regulated RNA levels in the upregulated gene set is likely complex. Roles for gene body methylation include altered rates of splicing, alternative splicing, and expression of noncoding RNAs (62).

In sum, EBV infection of immortalized oral keratinocytes resulted in epigenetic alterations affecting the differentiation state, transcriptional profiles, and DNA methylation patterns of EBV-positive and transiently infected clones. Whether EBV manipulation of the host machinery is inadvertent due to activation of epigenetic remodelers acting on the viral episome or targeted as a mechanism to provide a cellular environment conducive for viral persistence is a key question that still needs to be answered. In this study, we have focused on common changes in DNA methylation and gene expression in support of targeted epigenetic alterations following EBV infection. We did observe heterogeneity in DNA methylation patterns and gene expression among clones that argues for a stochastic process in the acquisition of epigenetic alterations. Evident is the notion that EBV infection is able to reshuffle the cellular epigenome, resulting in long-lasting cellular consequences that can act as a viral mechanism for "hit-and-run" oncogenesis.

ACKNOWLEDGMENTS

We thank Paula Polk for microarray support, Shannon Mumphrey for flow cytometry support, and Yali Jia and Joseph Guidry for technical support.

This work was supported by grants from National Institute of General Medical Sciences (GM103433), National Cancer Institute (CA114416-01A2), and the Louisiana Board of Regents [LEQSF (2012-15)-RD-A-15].

REFERENCES

1. **Murray RJ, Kurilla MG, Brooks JM, Thomas WA, Rowe M, Kieff E, Rickinson AB.** 1992. Identification of target antigens for the human cytotoxic T cell response to Epstein-Barr virus (EBV): implications for the immune control of EBV-positive malignancies. J. Exp. Med. **176:**157–168. http://dx.doi.org/10.1084/jem.176.1.157.
2. **Arvey A, Tempera I, Tsai K, Chen HS, Tikhmyanova N, Klichinsky M, Leslie C, Lieberman PM.** 2012. An atlas of the Epstein-Barr virus transcriptome and epigenome reveals host-virus regulatory interactions. Cell Host Microbe **12:**233–245. http://dx.doi.org/10.1016/j.chom.2012.06.008.
3. **Tao Q, Robertson KD.** 2003. Stealth technology: how Epstein-Barr virus utilizes DNA methylation to cloak itself from immune detection. Clin. Immunol. **109:**53–63. http://dx.doi.org/10.1016/S1521-6616(03)00198-0.
4. **Tempera I, Lieberman PM.** 2014. Epigenetic regulation of EBV persistence and oncogenesis. Semin. Cancer Biol. **26:**22–29. http://dx.doi.org/10.1016/j.semcancer.2014.01.003.
5. **Johannsen E, Luftig M, Chase MR, Weicksel S, Cahir-McFarland E, Illanes D, Sarracino D, Kieff E.** 2004. Proteins of purified Epstein-Barr virus. Proc. Natl. Acad. Sci. U. S. A. **101:**16286–16291. http://dx.doi.org/10.1073/pnas.0407320101.
6. **Kalla M, Schmeinck A, Bergbauer M, Pich D, Hammerschmidt W.** 2010. AP-1 homolog BZLF1 of Epstein-Barr virus has two essential functions dependent on the epigenetic state of the viral genome. Proc. Natl. Acad. Sci. U. S. A. **107:**850–855. http://dx.doi.org/10.1073/pnas.0911948107.
7. **Masucci MG, Contreras-Salazar B, Ragnar E, Falk K, Minarovits J, Ernberg I, Klein G.** 1989. 5-Azacytidine up regulates the expression of Epstein-Barr virus nuclear antigen 2 (EBNA-2) through EBNA-6 and latent membrane protein in the Burkitt's lymphoma line Rael. J. Virol. **63:**3135–3141.
8. **Schaefer BC, Woisetschlaeger M, Strominger JL, Speck SH.** 1991. Exclusive expression of Epstein-Barr virus nuclear antigen 1 in Burkitt lymphoma arises from a third promoter, distinct from the promoters used in latently infected lymphocytes. Proc. Natl. Acad. Sci. U. S. A. **88:**6550–6554. http://dx.doi.org/10.1073/pnas.88.15.6550.
9. **Hino R, Uozaki H, Murakami N, Ushiku T, Shinozaki A, Ishikawa S, Morikawa T, Nakaya T, Sakatani T, Takada K, Fukayama M.** 2009.

Activation of DNA methyltransferase 1 by EBV latent membrane protein 2A leads to promoter hypermethylation of PTEN gene in gastric carcinoma. Cancer Res. **69:**2766–2774. http://dx.doi.org/10.1158/0008-5472.CAN-08-3070.

10. **Tsai CN, Tsai CL, Tse KP, Chang HY, Chang YS.** 2002. The Epstein-Barr virus oncogene product, latent membrane protein 1, induces the downregulation of E-cadherin gene expression via activation of DNA methyltransferases. Proc. Natl. Acad. Sci. U. S. A. **99:**10084–10089. http://dx.doi.org/10.1073/pnas.152059399.
11. **Bhende PM, Seaman WT, Delecluse HJ, Kenney SC.** 2004. The EBV lytic switch protein, Z, preferentially binds to and activates the methylated viral genome. Nat. Genet. **36:**1099–1104. http://dx.doi.org/10.1038/ng1424.
12. **Flower K, Thomas D, Heather J, Ramasubramanyan S, Jones S, Sinclair AJ.** 2011. Epigenetic control of viral life-cycle by a DNA-methylation dependent transcription factor. PLoS One **6:**e25922. http://dx.doi.org/10.1371/journal.pone.0025922.
13. **Tempera I, Wiedmer A, Dheekollu J, Lieberman PM.** 2010. CTCF prevents the epigenetic drift of EBV latency promoter Qp. PLoS Pathog. **6:**e1001048. http://dx.doi.org/10.1371/journal.ppat.1001048.
14. **Niller HH, Wolf H, Minarovits J.** 2011. Viral hit and run-oncogenesis: genetic and epigenetic scenarios. Cancer Lett. **305:**200–217. http://dx.doi.org/10.1016/j.canlet.2010.08.007.
15. **Iizasa H, Nanbo A, Nishikawa J, Jinushi M, Yoshiyama H.** 2012. Epstein-Barr Virus (EBV)-associated gastric carcinoma. Viruses **4:**3420–3439. http://dx.doi.org/10.3390/v4123420.
16. **Kim J, Lee HS, Bae SI, Lee YM, Kim WH.** 2005. Silencing and CpG island methylation of GSTP1 is rare in ordinary gastric carcinomas but common in Epstein-Barr virus-associated gastric carcinomas. Anticancer Res. **25:**4013–4019.
17. **Kwong J, Lo KW, To KF, Teo PM, Johnson PJ, Huang DP.** 2002. Promoter hypermethylation of multiple genes in nasopharyngeal carcinoma. Clin. Cancer Res. **8:**131–137.
18. **Lo KW, Chung GT, To KF.** 2012. Deciphering the molecular genetic basis of NPC through molecular, cytogenetic, and epigenetic approaches. Semin. Cancer Biol. **22:**79–86. http://dx.doi.org/10.1016/j.semcancer.2011.12.011.
19. **Matsusaka K, Kaneda A, Nagae G, Ushiku T, Kikuchi Y, Hino R, Uozaki H, Seto Y, Takada K, Aburatani H, Fukayama M.** 2011. Classification of Epstein-Barr virus-positive gastric cancers by definition of DNA methylation epigenotypes. Cancer Res. **71:**7187–7197. http://dx.doi.org/10.1158/0008-5472.CAN-11-1349.
20. **Saito M, Nishikawa J, Okada T, Morishige A, Sakai K, Nakamura M, Kiyotoki S, Hamabe K, Okamoto T, Oga A, Sasaki K, Suehiro Y, Hinoda Y, Sakaida I.** 2013. Role of DNA methylation in the development of Epstein-Barr virus-associated gastric carcinoma. J. Med. Virol. **85:**121–127. http://dx.doi.org/10.1002/jmv.23405.
21. **Tsao SW, Tsang CM, Pang PS, Zhang G, Chen H, Lo KW.** 2012. The biology of EBV infection in human epithelial cells. Semin. Cancer Biol. **22:**137–143. http://dx.doi.org/10.1016/j.semcancer.2012.02.004.
22. **Tsai CL, Li HP, Lu YJ, Hsueh C, Liang Y, Chen CL, Tsao SW, Tse KP, Yu JS, Chang YS.** 2006. Activation of DNA methyltransferase 1 by EBV LMP1 Involves c-Jun NH(2)-terminal kinase signaling. Cancer Res. **66:**11668–11676. http://dx.doi.org/10.1158/0008-5472.CAN-06-2194.
23. **Paschos K, Parker GA, Watanatanasup E, White RE, Allday MJ.** 2012. BIM promoter directly targeted by EBNA3C in polycomb-mediated repression by EBV. Nucleic Acids Res. **40:**7233–7246. http://dx.doi.org/10.1093/nar/gks391.
24. **Skalska L, White RE, Franz M, Ruhmann M, Allday MJ.** 2010. Epigenetic repression of p16(INK4A) by latent Epstein-Barr virus requires the interaction of EBNA3A and EBNA3C with CtBP. PLoS Pathog. **6:**e1000951. http://dx.doi.org/10.1371/journal.ppat.1000951.
25. **White RE, Groves IJ, Turro E, Yee J, Kremmer E, Allday MJ.** 2010. Extensive co-operation between the Epstein-Barr virus EBNA3 proteins in the manipulation of host gene expression and epigenetic chromatin modification. PLoS One **5:**e13979. http://dx.doi.org/10.1371/journal.pone.0013979.
26. **Hansen KD, Sabunciyan S, Langmead B, Nagy N, Curley R, Klein G, Klein E, Salamon D, Feinberg AP.** 2014. Large-scale hypomethylated blocks associated with Epstein-Barr virus-induced B-cell immortalization. Genome Res. **24:**177–184. http://dx.doi.org/10.1101/gr.157743.113.
27. **Hernando H, Shannon-Lowe C, Islam AB, Al-Shahrour F, Rodriguez-Ubreva J, Rodriguez-Cortez VC, Javierre BM, Mangas C, Fernandez AF, Parra M, Delecluse HJ, Esteller M, Lopez-Granados E, Fraga MF, Lopez-Bigas N, Ballestar E.** 2013. The B cell transcription program mediates hypomethylation and overexpression of key genes in Epstein-Barr virus-associated proliferative conversion. Genome Biol. **14:**R3. http://dx.doi.org/10.1186/gb-2013-14-1-r3.
28. **Anderton JA, Bose S, Vockerodt M, Vrzalikova K, Wei W, Kuo M, Helin K, Christensen J, Rowe M, Murray PG, Woodman CB.** 2011. The H3K27me3 demethylase, KDM6B, is induced by Epstein-Barr virus and over-expressed in Hodgkin's lymphoma. Oncogene **30:**2037–2043. http://dx.doi.org/10.1038/onc.2010.579.
29. **Leonard S, Wei W, Anderton J, Vockerodt M, Rowe M, Murray PG, Woodman CB.** 2011. Epigenetic and transcriptional changes which follow Epstein-Barr virus infection of germinal center B cells and their relevance to the pathogenesis of Hodgkin's lymphoma. J. Virol. **85:**9568–9577. http://dx.doi.org/10.1128/JVI.00468-11.
30. **Queen KJ, Shi M, Zhang F, Cvek U, Scott RS.** 2013. Epstein-Barr virus-induced epigenetic alterations following transient infection. Int. J. Cancer **132:**2076–2086. http://dx.doi.org/10.1002/ijc.27893.
31. **Molesworth SJ, Lake CM, Borza CM, Turk SM, Hutt-Fletcher LM.** 2000. Epstein-Barr virus gH is essential for penetration of B cells but also plays a role in attachment of virus to epithelial cells. J. Virol. **74:**6324–6332. http://dx.doi.org/10.1128/JVI.74.14.6324-6332.2000.
32. **Dirks W, Dexler H.** 2004. Authentication of cancer cell lines by DNA fingerprinting. Methods Mol. Med. **88:**43–55.
33. **Repic AM, Shi M, Scott RS, Sixbey JW.** 2010. Augmented latent membrane protein 1 expression from Epstein-Barr virus episomes with minimal terminal repeats. J. Virol. **84:**2236–2244. http://dx.doi.org/10.1128/JVI.01972-09.
34. **Morrison JA, Raab-Traub N.** 2005. Roles of the ITAM and PY motifs of Epstein-Barr virus latent membrane protein 2A in the inhibition of epithelial cell differentiation and activation of β-catenin signaling. J. Virol. **79:**2375–2382. http://dx.doi.org/10.1128/JVI.79.4.2375-2382.2005.
35. **Lin Z, Wang X, Strong MJ, Concha M, Baddoo M, Xu G, Baribault C, Fewell C, Hulme W, Hedges D, Taylor CM, Flemington EK.** 2013. Whole-genome sequencing of the Akata and Mutu Epstein-Barr virus strains. J. Virol. **87:**1172–1182. http://dx.doi.org/10.1128/JVI.02517-12.
36. **Krzywinski M, Schein J, Birol I, Connors J, Gascoyne R, Horsman D, Jones SJ, Marra MA.** 2009. Circos: an information aesthetic for comparative genomics. Genome Res. **19:**1639–1645. http://dx.doi.org/10.1101/gr.092759.109.
37. **Imai S, Koizumi S, Sugiura M, Tokunaga M, Uemura Y, Yamamoto N, Tanaka S, Sato E, Osato T.** 1994. Gastric carcinoma: monoclonal epithelial malignant cells expressing Epstein-Barr virus latent infection protein. Proc. Natl. Acad. Sci. U. S. A. **91:**9131–9135. http://dx.doi.org/10.1073/pnas.91.19.9131.
38. **Feederle R, Neuhierl B, Bannert H, Geletneky K, Shannon-Lowe C, Delecluse HJ.** 2007. Epstein-Barr virus B95.8 produced in 293 cells shows marked tropism for differentiated primary epithelial cells and reveals interindividual variation in susceptibility to viral infection. Int. J. Cancer **121:**588–594. http://dx.doi.org/10.1002/ijc.22727.
39. **Pegtel DM, Middeldorp J, Thorley-Lawson DA.** 2004. Epstein-Barr virus infection in ex vivo tonsil epithelial cell cultures of asymptomatic carriers. J. Virol. **78:**12613–12624. http://dx.doi.org/10.1128/JVI.78.22.12613-12624.2004.
40. **Dawson CW, Dawson J, Jones R, Ward K, Young LS.** 1998. Functional differences between BHRF1, the Epstein-Barr virus-encoded Bcl-2 homologue, and Bcl-2 in human epithelial cells. J. Virol. **72:**9016–9024.
41. **Dawson CW, Rickinson AB, Young LS.** 1990. Epstein-Barr virus latent membrane protein inhibits human epithelial cell differentiation. Nature **344:**777–780. http://dx.doi.org/10.1038/344777a0.
42. **Scholle F, Bendt KM, Raab-Traub N.** 2000. Epstein-Barr virus LMP2A transforms epithelial cells, inhibits cell differentiation, and activates Akt. J. Virol. **74:**10681–10689. http://dx.doi.org/10.1128/JVI.74.22.10681-10689.2000.
43. **Boyce ST, Ham RG.** 1983. Calcium-regulated differentiation of normal human epidermal keratinocytes in chemically defined clonal culture and serum-free serial culture. J. Investig. Dermatol. **81:**33s-40s. http://dx.doi.org/10.1111/1523-1747.ep12540422.
44. **Matter K, Aijaz S, Tsapara A, Balda MS.** 2005. Mammalian tight junctions in the regulation of epithelial differentiation and proliferation. Curr. Opin. Cell Biol. **17:**453–458. http://dx.doi.org/10.1016/j.ceb.2005.08.003.
45. **Green H, Rheinwald JG, Sun TT.** 1977. Properties of an epithelial cell type in culture: the epidermal keratinocyte and its dependence on products of the fibroblast. Prog. Clin. Biol. Res. **17:**493–500.

46. **Krebs A, Frontini M, Tora L.** 2008. GPAT: retrieval of genomic annotation from large genomic position datasets. BMC Bioinformatics **9:**533. http://dx.doi.org/10.1186/1471-2105-9-533.
47. **Kwok WK, Pang JC, Lo KW, Ng HK.** 2009. Role of the RARRES1 gene in nasopharyngeal carcinoma. Cancer Genet. Cytogenet. **194:**58–64. http://dx.doi.org/10.1016/j.cancergencyto.2009.06.005.
48. **Wille CK, Nawandar DM, Panfil AR, Ko MM, Hagemeier SR, Kenney SC.** 2013. Viral genome methylation differentially affects the ability of BZLF1 versus BRLF1 to activate Epstein-Barr virus lytic gene expression and viral replication. J. Virol. **87:**935–950. http://dx.doi.org/10.1128/JVI.01790-12.
49. **Han J, Kamber M.** 2001. Data mining: concepts and techniques. Academic Press, London, United Kingdom.
50. **Pearson K.** 1901. On lines and planes of closest fit to systems of points in space. Philos. Mag. **2:**559–572. http://dx.doi.org/10.1080/14786440109462720.
51. **Wullaert A, Bonnet MC, Pasparakis M.** 2011. NF-κB in the regulation of epithelial homeostasis and inflammation. Cell Res. **21:**146–158. http://dx.doi.org/10.1038/cr.2010.175.
52. **Barbieri CE, Pietenpol JA.** 2006. p63 and epithelial biology. Exp. Cell Res. **312:**695–706. http://dx.doi.org/10.1016/j.yexcr.2005.11.028.
53. **Candi E, Cipollone R, Rivetti di Val Cervo P, Gonfloni S, Melino G, Knight R.** 2008. p63 in epithelial development. Cell. Mol. Life Sci. **65:**3126–3133. http://dx.doi.org/10.1007/s00018-008-8119-x.
54. **Israel A.** 2010. The IKK complex, a central regulator of NF-κB activation. Cold Spring Harb. Perspect. Biol. **2:**a000158. http://dx.doi.org/10.1101/cshperspect.a000158.
55. **Fotheringham JA, Mazzucca S, Raab-Traub N.** 2010. Epstein-Barr virus latent membrane protein-2A-induced ΔNp63α expression is associated with impaired epithelial-cell differentiation. Oncogene **29:**4287–4296. http://dx.doi.org/10.1038/onc.2010.175.
56. **Jones PA.** 2012. Functions of DNA methylation: islands, start sites, gene bodies and beyond. Nat. Rev. Genet. **13:**484–492. http://dx.doi.org/10.1038/nrg3230.
57. **Irizarry RA, Ladd-Acosta C, Wen B, Wu Z, Montano C, Onyango P, Cui H, Gabo K, Rongione M, Webster M, Ji H, Potash JB, Sabunciyan S, Feinberg AP.** 2009. The human colon cancer methylome shows similar hypo- and hypermethylation at conserved tissue-specific CpG island shores. Nat. Genet. **41:**178–186. http://dx.doi.org/10.1038/ng.298.
58. **Dihal AA, Boot A, van Roon EH, Schrumpf M, Farina-Sarasqueta A, Fiocco M, Zeestraten EC, Kuppen PJ, Morreau H, van Wezel T, Boer JM.** 2013. The homeobox gene MEIS1 is methylated in BRAF (p.V600E) mutated colon tumors. PLoS One **8:**e79898. http://dx.doi.org/10.1371/journal.pone.0079898.
59. **Oleksiewicz U, Liloglou T, Tasopoulou KM, Daskoulidou N, Bryan J, Gosney JR, Field JK, Xinarianos G.** 2013. Cytoglobin has bimodal: tumour suppressor and oncogene functions in lung cancer cell lines. Hum. Mol. Genet. **22:**3207–3217. http://dx.doi.org/10.1093/hmg/ddt174.
60. **Li L, Su X, Choi GC, Cao Y, Ambinder RF, Tao Q.** 2012. Methylation profiling of Epstein-Barr virus immediate-early gene promoters, BZLF1 and BRLF1 in tumors of epithelial, NK- and B-cell origins. BMC Cancer **12:**125. http://dx.doi.org/10.1186/1471-2407-12-125.
61. **Ohm JE, McGarvey KM, Yu X, Cheng L, Schuebel KE, Cope L, Mohammad HP, Chen W, Daniel VC, Yu W, Berman DM, Jenuwein T, Pruitt K, Sharkis SJ, Watkins DN, Herman JG, Baylin SB.** 2007. A stem cell-like chromatin pattern may predispose tumor suppressor genes to DNA hypermethylation and heritable silencing. Nat. Genet. **39:**237–242. http://dx.doi.org/10.1038/ng1972.
62. **Kulis M, Queiros AC, Beekman R, Martin-Subero JI.** 2013. Intragenic DNA methylation in transcriptional regulation, normal differentiation and cancer. Biochim. Biophys. Acta **1829:**1161–1174. http://dx.doi.org/10.1016/j.bbagrm.2013.08.001.